JOURNAL OF PETROLOGY | VOLUME 47 | NUMBER 10 | PAGES 1943–1971 | 2006 | doi:10.1093/petrology/egl032

Exhumation History of a Garnet Pyroxenite-bearing Mantle Section from a Continent–Ocean Transition (Northern Apennine Ophiolites, Italy)

A. MONTANINI[1]*, R. TRIBUZIO[2,3] AND R. ANCZKIEWICZ[4†]

[1]DIPARTIMENTO DI SCIENZE DELLA TERRA, UNIVERSITÀ DI PARMA, PARCO AREA DELLE SCIENZE 157A, 43100 PARMA, ITALY

[2]DIPARTIMENTO DI SCIENZE DELLA TERRA, UNIVERSITÀ DI PAVIA, I-27100 PAVIA, ITALY

[3]IGG-CNR ISTITUTO DI GEOSCIENZE E GEORISORSE, PAVIA, I-27100 PAVIA, ITALY

[4]DEPARTMENT OF GEOLOGY, ROYAL HOLLOWAY, UNIVERSITY OF LONDON, TW20 0EX EGHAM, UK

RECEIVED JUNE 2, 2005; ACCEPTED MAY 17, 2006; ADVANCE ACCESS PUBLICATION JUNE 20, 2006

Garnet clinopyroxenite and garnet websterite layers occur locally within mantle peridotite bodies from the External Liguride Jurassic ophiolites (Northern Apennines, Italy). These ophiolites were derived from an ocean–continent transition similar to the present-day western Iberian margin. The garnet clinopyroxenites are mafic rocks with a primary mineral assemblage of pyrope-rich garnet + sodic Al-augite (Na_2O ~2·5 wt %, Al_2O_3 ~12·5 wt %), with accessory graphite, Fe–Ni sulphides and rutile. Decompression caused Na-rich plagioclase ($An_{50–45}$) exsolution in clinopyroxene porphyroclasts and extensive development of symplectites composed of secondary orthopyroxene + plagioclase ($An_{85–72}$) + Al-spinel ± clinopyroxene ± ilmenite at the interface between garnet and primary clinopyroxene. Further decompression is recorded by the development of an olivine + plagioclase-bearing assemblage, locally under syn-kinematic conditions, at the expense of two-pyroxenes + Al-spinel. Mg-rich garnet has been also found in the websterite layers, which are commonly characterized by the occurrence of symplectites made of orthopyroxene + Al-spinel ± clinopyroxene. The enclosing peridotites are Ti-amphibole-bearing lherzolites with a fertile geochemical signature and a widespread plagioclase-facies mylonitic foliation, which preserve in places a spinel tectonite fabric. Lu–Hf and Sm–Nd mineral isochrons (220 ± 13 Ma and 186.0 ± 1·8 Ma, respectively) have been obtained from a garnet clinopyroxenite layer and interpreted as cooling ages. Geothermobarometric estimates for the high-pressure equilibration have yielded T ~1100°C and P ~2·8 GPa. The early decompression was associated with moderate cooling, corresponding to T ~950°, and development of a spinel tectonite fabric in the lherzolites. Further decompression associated with plagioclase–olivine growth in both peridotites and pyroxenites was nearly isothermal. The shallow evolution occurred under a brittle regime and led to the superposition of hornblende to serpentine veining stages. The garnet pyroxenite-bearing mantle from the External Liguride ophiolites represents a rare tectonic sampling of deep levels of subcontinental lithosphere exhumed in an oceanic setting. The exhumation was probably accomplished through a two-step process that started during Late Palaeozoic continental extension. The low-pressure portion of the exhumation path, probably including also the plagioclase mylonitic shear zones, was related to the Mesozoic (Triassic to Jurassic) rifting that led to continental break-up. In Jurassic times, the studied mantle sequence became involved in an extensional detachment process that resulted in sea-floor denudation.

KEY WORDS: *garnet pyroxenite; ophiolite; non-volcanic margin; mantle exhumation; Sm–Nd and Lu–Hf geochronology*

INTRODUCTION

The architecture and tectonic evolution of non-volcanic continental margins have been extensively investigated

*Corresponding author. E-mail: alessandra.montanini@unipr.it.
†Present address: Polish Academy of Sciences, Krakow Research Centre, Krakow, Poland.

in the last two decades in the western Iberian margin (e.g. Boillot *et al.*, 1989; Beslier *et al.*, 1996; Whitmarsh *et al.*, 2001). These studies have shown the existence of a characteristic zone of exhumed continental mantle, between continent and newly formed oceanic crust. The record of Ligurian Tethys ophiolites [here taking 'ophiolite' as a descriptive term to denote an association of peridotites with mid-ocean ridge (MOR)-type gabbros, basalt lavas and pelagic sediments] from the Alpine belt has provided fundamental clues about the nature of this continent–ocean transition (e.g. Bertotti *et al.*, 1993; Manatschal & Bernoulli 1999; Desmurs *et al.*, 2001; Manatschal *et al.*, 2001; Müntener & Hermann, 2001).

Recent studies have proposed that extension leading to final continental break-up is accommodated through different fault systems (Whitmarsh *et al.*, 2001; Manatschal, 2004) and showed that exhumation at the sea floor of the subcontinental mantle is a late process accomplished through relatively shallow downward concave faults. Petrological studies demonstrated the effects of the interaction between rising asthenospheric melts and lithospheric mantle rocks, and suggested that these processes played a significant role in modifying the lithospheric rheology, influencing the localization of continental rupture and the onset of sea-floor spreading (Müntener & Piccardo, 2003). However, geochronological constraints on the timing of mantle evolution during rifting are commonly lacking and little is known about the timing of high-temperature structures observed within the exhumed mantle rocks. The involvement of deep levels of subcontinental mantle during the rifting stages that precede the formation of an oceanic basin still remains an open issue.

The opening of the Ligurian Tethys in Middle Jurassic times led to the separation of the continental plates of Europe and Adria and gave rise to uplift and denudation of subcontinental lithospheric mantle, which is at present exposed in the Alpine chain. Some of these mantle bodies were affected by thermochemical erosion and refertilization processes related to asthenospheric upwelling during rifting and oceanization (Müntener & Piccardo, 2003), but rare occurrences of peridotites retaining their subcontinental origin are still preserved (e.g. Rampone *et al.*, 1995; Müntener *et al.*, 2004). New findings of garnet pyroxenite layers within ophiolitic mantle peridotites from the Northern Apennines provide an opportunity to throw light onto the evolution of subcontinental lithospheric mantle affected by extensional rift-related processes. This garnet pyroxenite-bearing mantle section is not contaminated by ascending asthenospheric melts and preserves relics of a deep-seated lithospheric history. Melting of garnet-bearing mafic rocks has been invoked to explain the 'garnet signature' of mid-ocean ridge basalt (MORB) (e.g. Hirschmann & Stolper, 1996) and of isotopically enriched MORB compositions (Salters & Dick, 2001). However, garnet pyroxenite layers are characteristic of mantle bodies exhumed in orogenic settings (e.g. Davies *et al.*, 1993; Pearson *et al.*, 1993). Garnet pyroxenites are absent in peridotite exposures on the present-day ocean floors and, to our knowledge, only two occurrences in ophiolitic mantle rocks have been reported (Peters, 1968; Müntener & Hermann, 1996; Blichert-Toft *et al.*, 1999).

To unravel the exhumation history of the garnet pyroxenite-bearing mantle from the Northern Apennines, we combine field, petrological and geochronological investigations. In particular, Sm–Nd and Lu–Hf mineral isochrons for a garnet pyroxenite allow us to constrain the age of the mantle uplift. The determination of the pressure–temperature–time evolution of this mantle section suggests that only the low-pressure portion of the exhumation path, probably including also the development of plagioclase-facies shear zones, is related to rifting and continental break-up leading to the opening of the Ligurian Tethys. We argue that this has implications for the general understanding of the processes leading to the opening of oceanic basins along non-volcanic margins.

GEOLOGICAL AND PETROLOGICAL FRAMEWORK

The Northern Apennine ophiolites are remnants of lithosphere from the Ligurian Tethys ocean, which opened in Middle Jurassic times (Lemoine *et al.*, 1987; Bill *et al.*, 2001). They occur in two distinct ophiolite-bearing tectonic units, ascribed to different palaeogeographical domains (Fig. 1). The Internal Liguride (IL) ophiolites have lithostratigraphic characteristics that have been related to an intra-oceanic setting, i.e. as on-land analogues of oceanic lithosphere that originated at slow-spreading centres (Barrett & Spooner, 1977; Cortesogno *et al.*, 1987; Tribuzio *et al.*, 2000). In the External Liguride units (EL), ophiolites consist of fertile lherzolites, MOR-type basalts and rare gabbroic rocks occurring as large olistoliths within Cretaceous sedimentary mélanges, together with rare continental crust bodies locally displaying primary relationships with the ophiolites (Marroni *et al.*, 1998). The gabbros have trace element and Nd–Sr isotope characteristics consistent with derivation from N-MORB magmas and their emplacement predated the oldest pelagic sediments of the Ligurian Tethys ophiolites (Tribuzio *et al.*, 2004), thus testifying to the occurrence of a syn-rift MOR-type magmatic activity. The association of continental crust with the ophiolites was attributed to their formation in a fossil ocean–continent transition zone (Marroni *et al.*, 1998), similar to that of modern non-volcanic

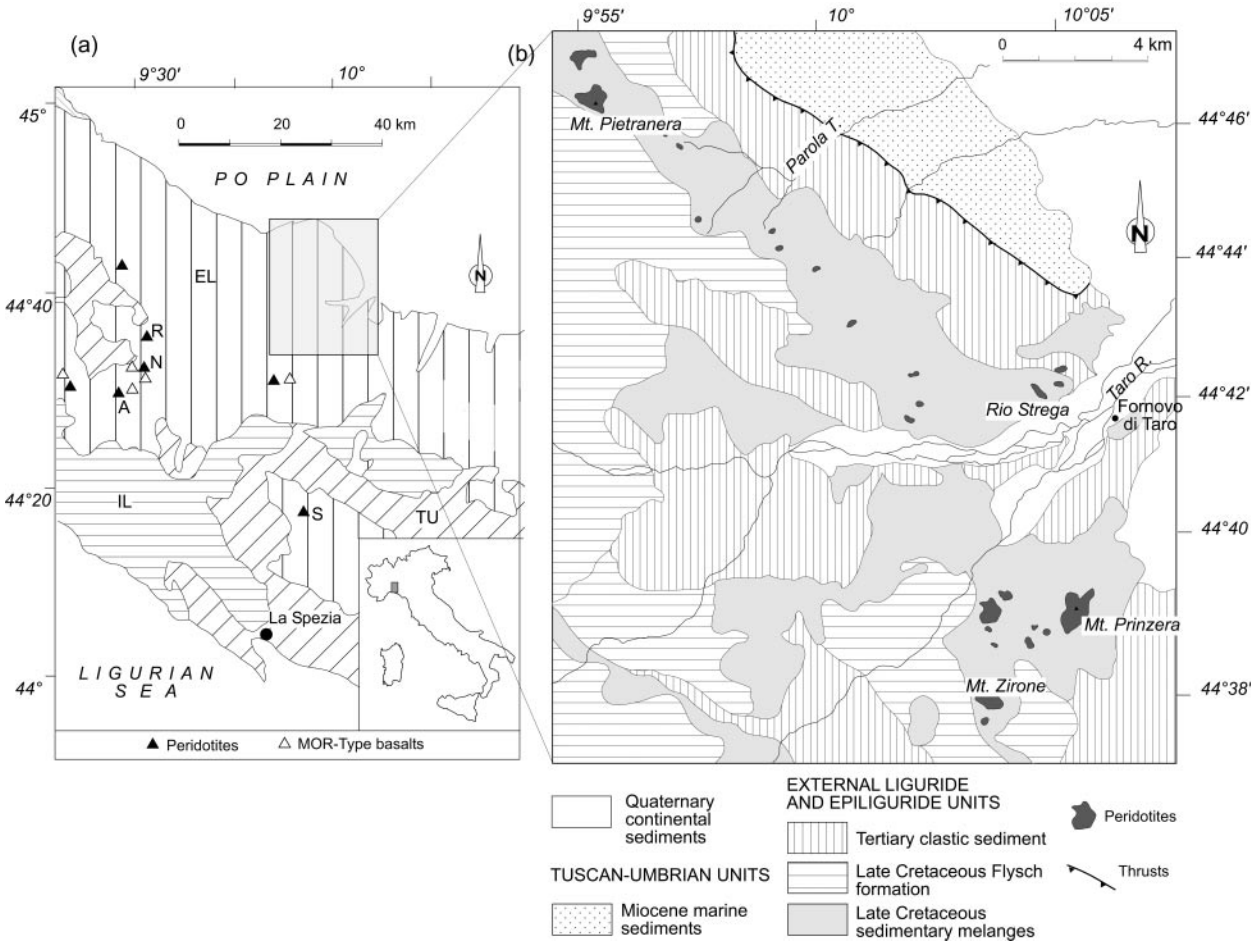

Fig. 1. (a) Tectonic sketch map of the Northern Apennines. Abbreviations for the tectonic units: TU, Tuscan–Umbrian units; IL, Internal Liguride Units; EL, External Liguride and Epiliguride Units; main peridotite outcrops are also reported: A, Mt. Aiona; N, Mt. Nero; S, Suvero; R, Mt. Ragola. (b) Simplified geological map of the investigated area.

continental margins. In particular, the External Liguride mantle rocks bear close petrological and geochemical similarities (Rampone & Piccardo, 2000; Tribuzio *et al.*, 2004) to those from the western Iberia margin (e.g. Boillot *et al.*, 1989; Whitmarsh *et al.*, 2001).

Detailed petrological and geochemical studies were carried out on mantle peridotite slide-blocks located in the southern sector of the External Liguride units (namely Suvero, Mt. Nero and Mt. Ragola massifs, Fig. 1). These peridotites are mainly spinel lherzolites with protogranular to tectonite fabrics, commonly displaying extensive growth of plagioclase (Piccardo, 1976; Beccaluva *et al.*, 1984; Piccardo *et al.*, 1990). These lherzolites contain disseminated Ti-rich amphibole and sporadic spinel pyroxenite layers. Temperature estimates for the spinel-facies equilibration (1000–1050°C) are compatible with continental geothermal gradients (Rampone *et al.*, 1995). The relatively fertile nature of the southern External Liguride peridotites is shown by high amounts of clinopyroxene (10–15 vol. %), high whole-rock Al_2O_3 contents and flat to slightly light rare earth element (LREE)-depleted clinopyroxene REE patterns (Rampone *et al.*, 1995). Nd–Sr–Os isotope investigations indicate a Proterozoic age for the accretion of the Suvero mantle body to the subcontinental lithosphere (see also Snow *et al.*, 2000). In addition, recent studies have indicated that the southern External Liguride peridotites were affected by refertilization by asthenospheric melts during the Ligurian Tethys formation (Piccardo *et al.*, 2004*a*, 2004*b*).

In the northern sector of the External Ligurides (Fig. 1), ophiolites are scarce and almost exclusively represented by the ultramafic rocks that form the basis of this study (Bernini *et al.*, 1997; Marroni *et al.*, 2002). These mantle rocks form several bodies embedded in a narrow, NW–SE-trending belt of sedimentary mélanges of Late Cretaceous age that crop out along the margin of the Northern Apennine chain close to the Po Plain. The enclosing sediments do not show any significant metamorphic recrystallization related to the

Alpine orogenic cycle. The mélange also includes rare MOR-type basalts (Montanini & Tribuzio, 2003) and fragments of continental crust (mafic granulites, amphibolites, granitoids). The ultramafic bodies are of variable size, ranging from only some tens of metres to a few kilometres (Fig. 1).

FIELD RELATIONS

The mantle peridotites commonly show a mylonitic fabric characterized by relatively large (up to 1 cm across) pyroxene porphyroclasts. A thickness of several hundred metres can be conservatively estimated for the studied mylonitic shear zones. The peridotites contain pyroxenite layers concordant with the foliation of the host peridotite, ranging in thickness from a few millimetres to ~2 m.

The garnet clinopyroxenite layers are, in the central part of the thickest layers, locally isotropic and coarse-grained. In such cases, the external portions of the garnet clinopyroxenite layers display a weak foliation defined by elongated clinopyroxene porphyroclasts. The isotropic rocks are composed of pinkish Al-augite and embayed red–orange garnets with greenish pyroxene–spinel coronas; clusters of tiny graphite flakes occur in places. Garnet-free layers with evident foliation are also present. These layers are fine-grained and dark grey, and show parallel millimetre-scale pyroxene-rich and olivine-rich bands, concordant with the main peridotite foliation.

The most common layers are represented by boudinaged pinkish grey medium- to fine-grained websterites, of 2–10 cm thickness. Websterites may contain thin stretched lenses of olivine. Interlayering of centimetre-scale websterite and olivine-rich bands is also common.

Brittle deformation with multiple stages of veining, hydration and the formation of tectonic breccias is widespread and shows similar patterns in the different mantle bodies. Both the earliest veining events (F_1 and F_2) yielded orthogonal fracture systems subparallel and normal to the mylonitic foliation. The oldest veins (F_1) are up to 2–3 mm thick and filled with dark green amphibole ± chlorite. F_2 veins have variable thickness (millimetre- to centimetre-sized) and are filled with white fibrous or massive dark green serpentine (± opaque minerals). Anastomosing F_2 veins are also locally present. In strongly foliated serpentinitized peridotites, there are locally millimetre- to centimetre-thick F_2 veins of light green massive serpentine or densely spaced subparallel millimetre-sized veinlets of fibrous white serpentine, both subparallel to the mylonitic foliation.

A brittle event (F_3) pervasively overprinted the former vein systems, yielding cohesive tectonic breccias ('jigsaw breccia'). These cataclasites consist of millimetre- to metre-sized angular clasts in a fine-grained, grey–bluish, serpentine matrix with little displacement and no significant rotation of the clasts, as attested to by the coherence of the mylonitic fabric and pyroxenite layer orientation between adjacent clasts. Carbonates are absent in the early vein generations, but they may occur as tiny spherules in the matrix of the jigsaw breccia. Multiple calcite vein generations, commonly associated with Fe-sulphides and massive green serpentine and/or talc, may crosscut the jigsaw breccia and bound the clasts, yielding ophicalcite-like rocks (e.g. Lemoine *et al.*, 1987; Treves & Harper, 1994).

PETROGRAPHY AND MICROSTRUCTURES

Garnet clinopyroxenites

The garnet clinopyroxenites are commonly affected by a complex retrograde evolution. In particular, retrogression can be divided into two distinct stages characterized, respectively, by two-pyroxene + spinel + plagioclase and olivine + plagioclase assemblages.

The high-pressure protoliths were characterized by a coarse-grained isotropic texture and an anhydrous bimineralic assemblage of garnet + clinopyroxene (Cpx I). The oldest clinopyroxene generation (Cpx I) is preserved only as inclusions in garnet. Accessory graphite, Fe–Ni–Cu sulphides and rutile have been found locally. Graphite occurs as small flakes and stacks of flakes with grain size up to 2–3 mm. No diamond pseudomorphs have been observed. Raman spectra (Montanini *et al.*, 2005) indicate a highly ordered structure similar to that of graphite crystallized at high temperature in peridotite and eclogite xenoliths (Pearson *et al.*, 1993). Sulphides may occur both as tiny (20–50 μm) inclusions in garnet or, locally, as interstitial, lobate larger crystals (0·1–1·0 mm).

Complex pyroxene–spinel–plagioclase symplectites are present at the interface between garnet and Cpx I (Fig. 2a). Fine-grained (μm-scale) radial and fibrous symplectites composed of orthopyroxene (Opx I) + green spinel (Spl I) + plagioclase ± ilmenite (Fig. 3a) occur at the rims of the garnet relics. This inner symplectite is commonly rimmed by coarser symplectitic intergrowths of the same minerals and, locally, by an outer shell of plagioclase + clinopyroxene (Cpx IIa) with vermicular spinel inclusions.

Coarse clinopyroxene grains (up to 4–5 mm; Cpx IIb) display plagioclase exsolution lamellae and occur as porphyroclasts in medium-grained granoblastic domains composed of clinopyroxene (Cpx III) + orthopyroxene (Opx II) + minor plagioclase and green spinel (Spl II; Fig. 2b). Several garnet clinopyroxenite layers are almost completely retrogressed to foliated rocks characterized by this latter assemblage, which locally preserves pyroxene–spinel symplectitic domains after garnet and

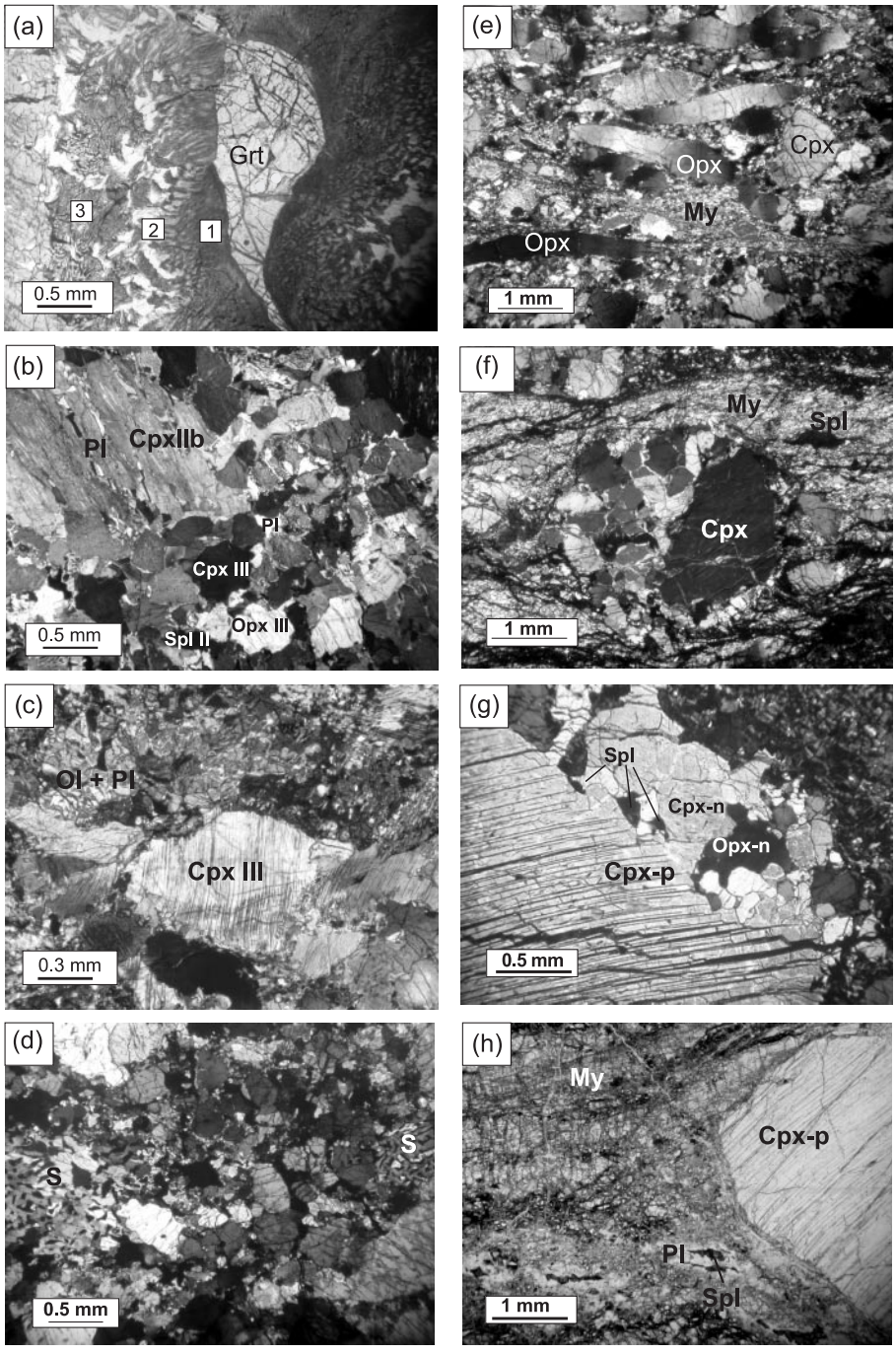

Fig. 2. Photomicrographs of garnet clinopyroxenites, websterites and peridotites. (a) Garnet clinopyroxenite: reaction corona around garnet (Grt) formed by radial Opx I + Spl I + Pl symplectites (1–2), coarsening outwards, and by an outer shell (3) of Cpx IIa + Spl + Pl (see text for further explanation); plane-polarized light (PPL). (b) Clinopyroxene porphyroclast (Cpx IIb) with exsolved plagioclase blebs in a recrystallized two-pyroxene domain (Cpx III + Opx III + Spl II + Pl) of a retrogressed garnet clinopyroxenite; cross-polarized light (CPL). (c) Olivine+ plagioclase symplectites and fine-grained olivine + plagioclase aggregates (Ol + Pl) rimming retrograde pyroxenes in a retrogressed garnet clinopyroxenite; CPL. (d) Orthopyroxene–clinopyroxene–spinel intergrowths (S) after garnet in a websterite; CPL. (e) Orthopyroxene porphyroclasts with high aspect ratio and fine-grained olivine + plagioclase-bearing matrix (My = ol + pl + cpx + opx) in highly deformed websterite; CPL. (f) Small spinel websterite boudin (recrystallized cpx + opx + spl + amph domain around a clinopyroxene porphyroclast, Cpx-p) in peridotite mylonite (My, fine-grained polyphase mylonite matrix of olivine + plagioclase + clinopyroxene + orthopyroxene); CPL. (g) Relic of spinel tectonite texture in peridotite: neoblastic ol + opx + cpx + spl around a large clinopyroxene porphyroclast (Cpx-p); PPL. (h) Plagioclase peridotite mylonite displaying small relict spinels (Spl) rimmed by plagioclase (Pl) and porphyroclast clinopyroxene (Cpx-p) mantled by a fine-grained polyphase mylonite matrix (My); PPL.

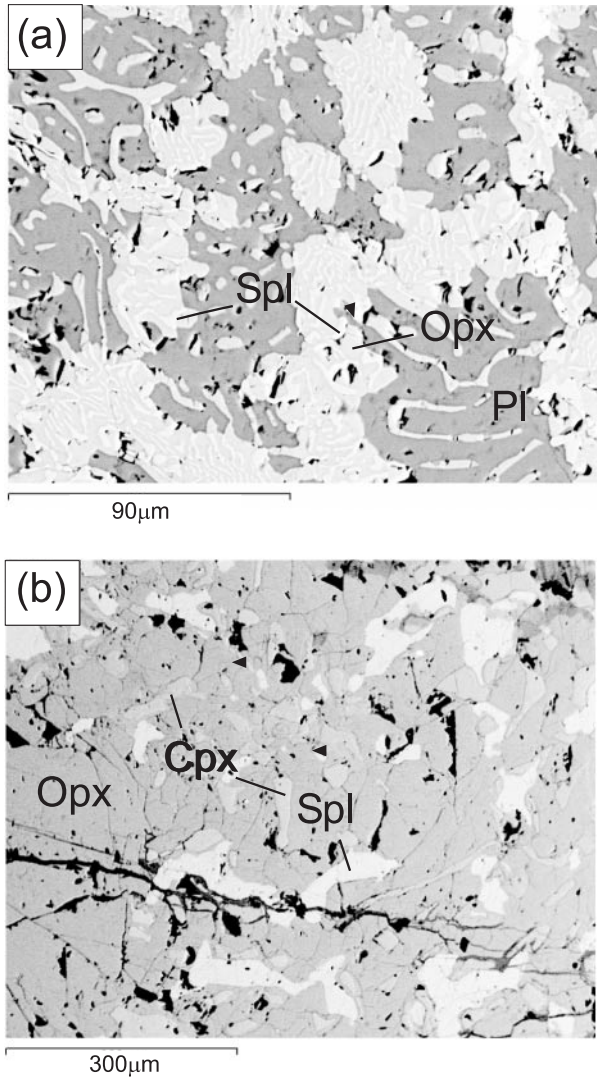

Fig. 3. BSE (back-scattered electron) images of fine-grained products after garnet + pyroxenes in garnet pyroxenites. (a) Orthopyroxene (Opx, light grey)–plagioclase (Pl, dark grey)–spinel (Spl, white) symplectites in the inner corona with a radial structure like that of Fig. 2a. (b) Orthopyroxene (Opx, dark grey) with vermicular spinel (Spl, light grey) and clinopyroxene (Cpx, medium grey) inclusions.

clinopyroxene IIb porphyroclasts showing breakdown to secondary clinopyroxene + plagioclase. In these rocks, small (1–2 mm) clinopyroxene and orthopyroxene grains (corresponding to Cpx III and Opx II) are rimmed by fine-grained neoblastic Cpx (IV) + Opx (III) + plagioclase + spinel (Spl III). The garnet textural domain is recognized by orthopyroxene including vermicular grains of spinel (locally with a thin rind of secondary plagioclase) and minor clinopyroxene (Fig. 3b).

An olivine + plagioclase (± Spl IV) assemblage occurs as fine-grained aggregates replacing either the pyroxene–plagioclase–spinel symplectites after garnet, or the garnet relics within the symplectites. The association of olivine + plagioclase is also found as coronas and/or symplectites (Fig. 2c) around pyroxenes at the contact with spinel. In a few layers, the olivine + plagioclase assemblage syn-kinematically overgrows pyroxene + spinel (II) + plagioclase domains, locally associated with trace amounts of Spl (IV) and brown amphibole.

The garnet clinopyroxenites do not record an extensive low-temperature hydration process. Veining and replacement of the pyroxene + spinel + plagioclase assemblage by pale green amphibole + chlorite related to the F_1 stage is locally observed. Serpentine F_2 veins and serpentine ± chlorite pseudomorphs after olivine occur in places.

Websterites

The websterites are medium-grained rocks consisting of clinopyroxene (40–60%), orthopyroxene (20–30%), spinel (5–10%), plagioclase (0–10%), olivine (0–5%) and brown amphibole (0–3%); Fe–Ni sulphides are common accessory minerals. The most common texture is protomylonitic, characterized by highly stretched, elongated orthopyroxene crystals with high aspect ratios (up to 15; Fig. 2f) and fine-grained neoblastic aggregates of orthopyroxene + clinopyroxene + spinel ± amphibole around pyroxene porphyroclasts. Evidence for a previous garnet-bearing assemblage comes from rounded domains composed of Opx + Cpx + Spl symplectites (Fig. 2d). In one case, we have found tiny garnet relics within these symplectites. Coarsening and progressive annealing of the symplectites after garnet led to the formation of pyroxene–spinel clusters and, locally, to aggregates with allotriomorphic texture (Fig. 2e and f).

The pyroxene + spinel assemblage is locally mantled by fine-grained olivine–plagioclase-rich mylonitic bands (Fig. 2e and f), similar to those occurring in the peridotite (see the next section). Strain localization associated with this deformation is commonly observed at the contact with peridotite. The clinopyroxene porphyroclasts frequently show plagioclase exsolution and rims. Green to greenish brown spinel occurs both as small rounded or vermicular grains within orthopyroxene and as larger allotriomorphic crystals, commonly rimmed by plagioclase. Olivine of probably primary origin occurs as irregularly shaped crystals or thin seams surrounded by pyroxenes similar to the 'olivine flames' of Burg *et al.* (1998). Secondary olivine forms: (1) radial crystals, associated with plagioclase + greenish brown spinel ± ilmenite ± brown amphibole, forming coronas between pyroxenes and green spinel, locally stretched along the main foliation; (2) granoblastic domains composed by the same phases; (3) fine-grained plagioclase-bearing (± brown amphibole) mylonitic bands.

Peridotites

The peridotites are clinopyroxene-rich (10–15 vol. %) spinel–plagioclase lherzolites with accessory brown amphibole. The oldest recognizable texture is preserved in small domains characterized by coarse-grained (up to 5–10 mm across) orthopyroxene and clinopyroxene grains surrounded by smaller polygonal or irregular-shaped neoblasts of olivine + pyroxene + spinel ± brown amphibole (Fig. 2g). These domains thus represent relics of a spinel-facies low-strain tectonite. Mutual pyroxene exsolution may occur in these porphyroclasts.

The spinel-facies assemblage is overprinted by plagioclase-facies recrystallization associated with the development of a mylonitic fabric. The mylonite microstructure is characterized by aligned porphyroclasts of pyroxene + brown spinel + brown amphibole and by an ultrafine-grained (~20–50 μm) polyphase aggregate composed of olivine + pyroxenes + plagioclase (± spinel ± accessory brown amphibole) occurring as millimetre-sized bands, lenses and porphyroclast tails (Fig. 2h). Crystals in this polyphase matrix commonly display grain boundary alignment parallel to the mylonitic foliation.

Orthopyroxene porphyroclasts may be rounded, lozenge-shaped or elongate along the mylonitic foliation with high aspect ratio (up to ~10). Clinopyroxene is usually more equant than orthopyroxene. Both pyroxenes commonly show evidence for intracrystalline deformation (i.e. undulose extinction, bending and kinking). Plagioclase occurs as (1) thin rims between spinel and pyroxene porphyroclasts, (2) tiny neoblastic grains in the mylonitic matrix and, rarely, (3) exsolution in clinopyroxene porphyroclasts.

The mylonitic foliation is locally crosscut by thin fractures filled with prismatic pale green amphibole, which is commonly associated with minor amounts of chlorite (F_1). Amphibole and chlorite also grow adjacent to the fractures, as pseudomorphs after clinopyroxene and brown amphibole, and as coronas around spinel, respectively (Fig. 4a).

The association of amphibole + chlorite is followed by multiple serpentine veining episodes (F_2), associated with serpentinization, to various extents, of the host rock. X-ray diffraction analyses have shown that lizardite is the dominant phase in the serpentinized peridotite. Vein serpentine may be fibrous with antiaxial filling or isotropic, rarely associated with magnetite. Olivine alteration is mainly accomplished through growth of 'mesh texture' serpentine (with frequent preservation of olivine cores) and, to a lesser extent, of 'hourglass' serpentine. Magnetite abundance in olivine pseudomorphs usually increases with increasing degree of serpentinization. Pyroxenes may be pseudomorphed by

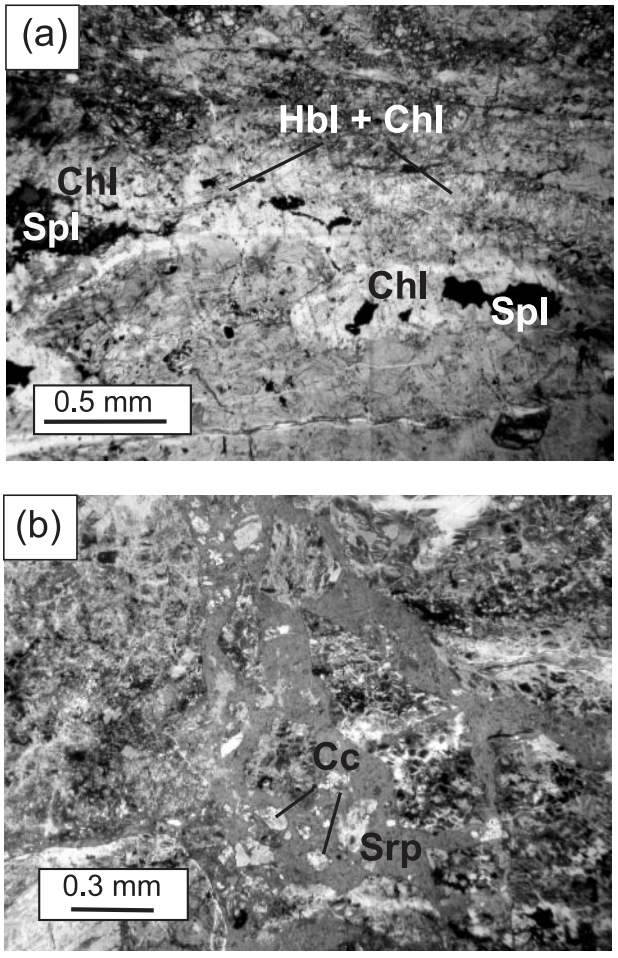

Fig. 4. Photomicrographs of retrogressed and hydrated peridotite textures. (a) Hornblende (Hbl) veins (F_1 stage) subparallel to the plagioclase mylonitic foliation defined by elongated spinels rimmed by chlorite (Chl); plane-polarized light (PPL). (b) Cataclasite (F_3 stage) formed by serpentinized peridotite clasts in a serpentine + calcite matrix; PPL.

light green or bluish fibrous serpentine ('bastite'). Relics of the former mantle assemblages, mainly represented by sparse brown spinel grains with opaque rims, are only rarely preserved in the serpentinized plagioclase mylonites. Two main types of subparallel veins follow the original plagioclase-bearing foliation: (1) thin ribbon lizardite veins (± magnetite seams) transected by (2) millimetre- to centimetre-thick massive lizardite veins with low birefringence and undulose extinction.

All the structures described above are pervasively disrupted by the F_3 stage of brecciation. These breccias show a jigsaw-puzzle pattern at both meso- and microscales, and show evidence for polyphase cracking and veining. The breccia matrix (Fig. 4b) is made of fine-grained serpentinite derived from comminution of the larger clasts and by yellow–light brown serpentine in tiny

fibrous–spherulitic aggregates. The serpentine matrix also contains clusters of micrometre-scale, curved needles of Ni-sulphide (millerite), and locally abundant calcite spherules, studded with dark fluid inclusions, some tenths of a micrometre across.

ANALYTICAL METHODS

Major element mineral analyses were obtained on samples representative of the different lithologies and different stages of retrograde evolution. Mineral analyses were performed at the Dipartimento di Scienze della Terra of Università di Parma using a JEOL-6400 electron microprobe equipped with LINK-ISIS energy-dispersive microanalytic system. Operating conditions were accelerating voltage of 15 kV and probe current of 0·25 nA; both natural minerals and synthetic compounds were used as standards. Trace amounts of Na_2O in garnet were analysed at CNR–Istituto di Geoscienze e Georisorse, Sezione di Firenze, using a JEOL JXA-8600 microprobe. Operating conditions were accelerating voltage of 15 kV, probe current of 100 nA and counting times of 20 s. These conditions provided a detection limit of ~40 ppm for Na.

Sm–Nd and Lu–Hf dating techniques were applied to a garnet clinopyroxenite layer (sample AM322). The rock was crushed and sieved to obtain a 150–250 μm fraction. Mineral concentrates were extracted using a Frantz magnetic separator and then purified by careful handpicking under a binocular microscope to obtain clinopyroxene, garnet and plagioclase separates, avoiding inclusion-bearing grains or small impurities derived from symplectitic intergrowths. Sm–Nd and Lu–Hf analyses of the garnet clinopyroxenite layer were carried out on the same mineral and whole-rock splits. Details of sample digestion and ion exchange chromatography were presented by Anczkiewicz *et al.* (2004). Mass spectrometry procedures follow Thirlwall & Anczkiewicz (2004). Total procedure analytical blanks for Hf and Nd were <30 pg. All elements were analysed in a static, hard extraction mode using the Royal Holloway IsoProbe®. All errors are 2SE and relate to the last significant digits, except for age errors, which are 95% confidence level. All measurements were conducted on a single day to minimize correction for secular variation in the static $^{176}Hf/^{177}Hf$ of JMC47. $^{147}Sm/^{144}Nd$ errors are 0·3%. Reproducibility of the Aldrich Nd standard on the day of analyses was $^{143}Nd/^{144}Nd = 0{\cdot}511388 \pm 11$ (2SD, $n = 4$). Daily variations in $^{143}Nd/^{144}Nd$ ratios were normalized to $^{143}Nd/^{144}Nd = 0{\cdot}511421$. $^{176}Lu/^{177}Hf$ errors are 0·5%; the JMC475 standard on the day of analysis yielded $0{\cdot}282173 \pm 6$ (2SD, $n = 3$). Daily variations in $^{176}Hf/^{177}Hf$ ratios were normalized to $^{176}Hf/^{177}Hf = 0{\cdot}282165$. Mass bias corrections were made using $^{146}Nd/^{144}Nd = 0{\cdot}7219$ and $^{179}Hf/^{177}Hf = 0{\cdot}7325$.

MINERAL CHEMISTRY

Garnet pyroxenites

Garnet compositions cover the range $Prp_{53–45}Alm_{29–38}Grs_{11–20}$, with only minor spessartine component (≤1·5 mol %, Table 1, Fig. 5). Cr_2O_3 contents do not exceed 0·25 wt %. The low TiO_2 (0·10–0·20 wt %) and Na_2O concentrations (≤0·02 wt %, confirmed by unpublished LA-ICP-MS analyses that yielded Na ~120 ppm) are comparable with those of the diamond-free Group II eclogites defined by McCandless & Gurney (1989). The bulk composition of the symplectitic intergrowths in retrogressed pyroxenites was determined by electron microprobe and is a pyrope-rich garnet composition (Table 1). However, the analyses contain an excess of MgO relative to garnet stoichiometry and high amounts of Na_2O, which may be related to involvement of olivine and primary clinopyroxene in the garnet breakdown reaction, respectively.

The oldest clinopyroxene (Cpx I) has up to 12·6 wt % Al_2O_3 and 2·7 wt % Na_2O. Recalculation of structural formulae gives high proportions of the Ca-Tschermak component (15–20 mol %) and moderate jadeite contents (10–16 mol %). The structural formulae do not display any cation deficiency requiring the presence of a Ca-Eskola component. Similar clinopyroxene compositions were reported for Group II garnet pyroxenites from Beni Bousera (Kornprobst *et al.*, 1990).

The different generations of retrograde clinopyroxene have lower amounts of the Ca-Tschermak and jadeitic component than Cpx I and define a negative correlation in a plot of Na_2O–Al_2O_3 (Fig. 6a). The latest pyroxenes (Cpx IV) have the lowest amounts of the Ca-Tschermak and jadeitic component. The composition of the coarse clinopyroxene porphyroclasts characterized by plagioclase exsolution (Cpx IIb) is highly variable, both for Al_2O_3 and Na_2O contents. In particular, Na_2O concentrations vary over a wide range (1·3–0·1 wt %), even within the same crystal, with the lowest values occurring close to the plagioclase lamellae and patches.

The $Mg/(Mg + Fe^{2+})$ ratios of clinopyroxene and orthopyroxene from the garnet clinopyroxenites span a wide range (0·73–0·90 and 0·71–0·88, respectively). Cr_2O_3 varies in the range 0·05–0·30 wt % in both pyroxenes. The lowest $Mg/(Mg + Fe^{2+})$ values are associated with the lowest Cr contents in both pyroxenes. The forsterite content of olivine (61–85 mol %) exhibits a rough positive correlation with the $Mg/(Mg + Fe^{2+})$ values of the pyroxenes.

Spinel does not show appreciable compositional variation between the different textural domains. It is highly aluminous and Cr-poor (Cr_2O_3 ≤1·5 wt %); the $Mg/(Mg + Fe^{2+})$ values vary between 50 and 75 (Table 1). The brown amphibole occurring in the

Table 1: Representative electron microprobe analyses of minerals in the garnet-clinopyroxenite layers

Mineral	SiO_2	TiO_2	Al_2O_3	Cr_2O_3	FeO*	MnO	MgO	CaO	Na_2O	K_2O	Total	Mg-no.	Cr-no.	An
Sample AM322—Rio Strega														
Primary garnet-bearing assemblage														
Grt (1)	41·36	0·21	21·90	0·23	15·11	0·26	14·68	6·84	0·01	—	100·60	0·659		
Grt (2)	39·94	0·17	21·58	0·10	19·02	0·56	11·71	6·35	n.a.	—	99·44	0·538		
Cpx I	49·25	1·00	12·24	0·12	5·34	0·04	11·52	18·22	2·30	—	100·00	0·798		
Garnet corona														
Opx I	51·97	—	3·31	—	18·12	0·35	25·37	0·48	—	—	99·60	0·74		
Pl	49·21	—	31·40	—	0·50	0·03	—	15·14	2·91	—	99·19			73
Spl I	—	0·11	61·32	0·38	23·34	0·62	13·46	—	—	—	99·22	0·54	0·004	
Cpx IIa	50·92	0·77	5·42	0·09	6·42	0·17	15·48	20·33	0·25		99·85	0·811		
Retrograde plagioclase–pyroxene–spinel assemblage														
Cpx II b	47·81	0·82	11·85	0·20	6·34	0·08	11·64	19·60	1·33	—	99·67	0·783		
Pl-e	54·87	—	27·50	—	0·23	0·02	—	10·74	5·87	—	99·23			50
Cpx III	50·76	0·80	5·61	—	7·59	0·14	14·66	20·27	0·47	—	100·30	0·789		
Opx II	53·03	0·29	2·55	0·09	17·85	0·34	25·47	0·79	—	—	100·41	0·728		
Spl II	—	0·12	61·00	1·30	24·30	0·25	12·42	—	—	—	99·39	0·5	0·015	
Pl	56·12	—	26·73	—	0·18	0·09	0·00	9·69	6·20	0·04	99·05			46
Ol-bearing clinopyroxene corona														
Ol	37·01	—	—	—	30·66	0·42	31·54	—	—	—	99·63	0·65		
Pl	54·80		27·70	—	—	—	—	10·94	5·64	—	99·08			52
Sample AM288a—Mt. Prinzera														
Symplectite after garnet														
Opx I	55·58	—	2·76	0·11	9·27	0·10	32·10	0·42	—	—	100·35	0·869		
Cpx IIa	51·40	0·11	4·56	0·22	3·68	0·05	15·40	22·70	0·89	—	99·01	0·881		
Spl I	—	0·11	64·67	1·43	14·05	—	20·23	—	—	—	100·49	0·76	0·015	
Bulk (3)	41·39	0·03	21·30	0·26	7·70	0·12	21·10	6·77	0·41	—	99·08			
Retrograde plagioclase–pyroxene–spinel assemblage														
Cpx III-c	48·77	0·32	11·33	0·32	5·02	0·16	12·43	20·34	0·90		99·60	0·815		
Cpx III-r	50·73	0·35	6·83	0·23	5·07	0·11	13·98	21·69	0·63		99·62	0·831		
Opx II-c	53·19	0·11	4·79	0·27	12·30	0·35	28·17	0·54	—	—	99·72	0·803		
Opx II-r	55·07	0·19	1·89	0·08	12·71	0·28	28·91	0·60	—	—	99·73	0·802		
Cpx IV	52·00	0·18	4·58	0·13	3·17	—	16·08	22·38	0·80	—	99·32	0·926		
Opx III	54·65	—	3·90	0·17	8·28	0·28	31·37	0·45	—	—	99·10	0·872		
Spl III	—	0·08	65·65	1·22	13·19	0·29	19·50	—	—	—	99·93	0·76	0·012	
Pl	48·10	0·07	31·90	—	0·34	0·06	0·05	16·27	2·45	—	99·24			79
Retrograde ol-bearing assemblage														
Ol	40·10	—	—	—	13·76	0·18	45·68	—	—	0·10	99·82	0·86		
Pl	47·50	—	32·10	—	0·27	—	0·11	16·31	2·55	—	98·84			77
Spl IVa	—	0·05	65·15	2·26	14·08	0·12	18·46	0·10	—	—	100·22	0·7	0·030	
Sample AM364—Mt. Zirone														
Retrograde olivine-bearing assemblage														
Pl	54·50	—	27·70	—	0·26	—	—	11·80	4·88	0·08	99·22			56
Ks	40·30	6·20	12·28	0·60	10·64	0·16	13·24	11·61	3·06	0·13	98·22	0·69		

*Total iron as Fe^{2+}.
Grt, garnet; Cpx, clinopyroxene; Spl, spinel; Pl, plagioclase; Ol, olivine; Ks, kaersutite. Garnet composition respectively from the internal (1) and external (2) part of a 2 m thick layer; (3) is a bulk symplectite composition. Mg-number = $Mg/(Mg + Fe^{2+})$; Cr-number = $Cr/(Cr + Al)$; An is anorthite mol %; c, core; r, rim; e, exsolution; —, not detected; n.a., not analysed.

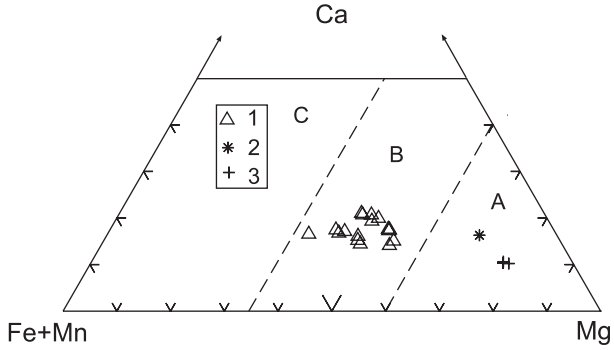

Fig. 5. Garnet composition in pyroxenite layers. 1, Garnet clinopyroxenites; 2, bulk symplectite composition in the retrogressed garnet clinopyroxenite AM288a; 3, websterite BA3. Dashed lines divide fields for Group A, B and C eclogite garnets (Taylor & Neal, 1989).

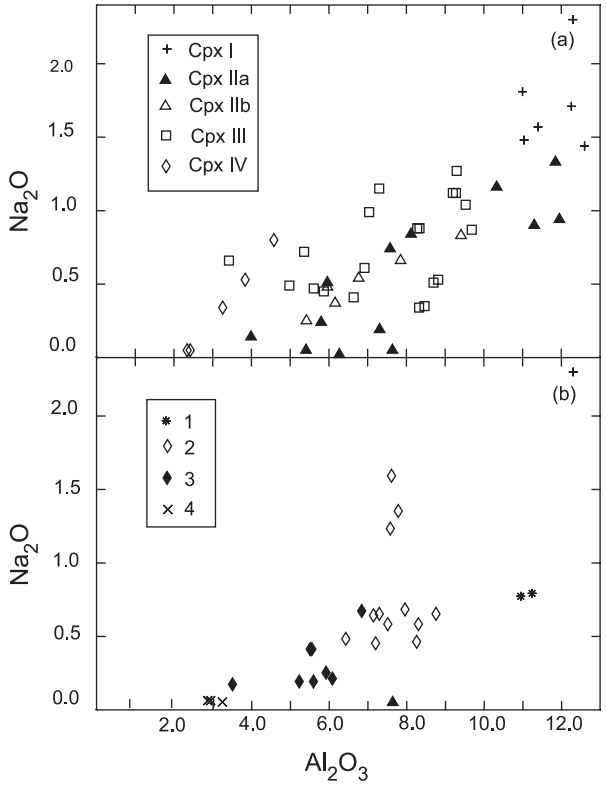

Fig. 6. Variation of Na_2O vs Al_2O_3 (wt %) for clinopyroxenes from pyroxenite layers. (a) Garnet clinopyroxenites (see text for further explanation of the different clinopyroxene generations); (b) websterites (1, Al_2O_3-rich porphyroclasts with plagioclase exsolution; 2, exsolution-free porphyroclasts; 3, neoblasts in spinel–pyroxene recrystallized domain; 4, neoblasts in mylonitic olivine-bearing bands).

olivine–plagioclase-bearing domains is kaersutite (Table 1).

The composition of plagioclase (Table 1) is controlled by textural position. Plagioclase from the Opx–Spl–Pl symplectites around garnet (Pl Ia) has high Ca contents (An = 68–85 mol %). Plagioclase lamellae within clinopyroxene (Pl Ib) and plagioclase grains in recrystallized two-pyroxene domains (Pl II) have 45–50 mol % anorthite.

Vein amphibole and amphibole overgrowths on clinopyroxene in the pyroxenitic layers is Mg-hornblende with high Al_2O_3 (up to 10·6 wt %) and Na_2O (1·6–2·2 wt %) contents, and low TiO_2 concentrations (0·13–0·25 wt %); significant amounts of Cl (~0·15 wt %; see Table 4) were detected. The associated chlorite is clinochlore, with Al_2O_3 and $Mg/(Mg + Fe^{2+})$ values of about 19 wt % and 0·88, respectively.

Websterites

Relict garnet has high pyrope (~78 mol %, Fig. 5) and Cr_2O_3 contents (~0·7 wt %), similar to the garnets from mantle lherzolites worldwide (Pearson & Nixon, 1996). Clinopyroxene porphyroclasts can have high amounts of Al_2O_3 (10–11 wt %) and Ca-Tschermak substitution (up to 18 mol %), whereas the jadeite component is low (≤6 mol %), probably as the result of exsolution of Na-rich plagioclase (An = 58 mol %; Fig. 6b). These clinopyroxenes are compositionally similar to Cpx IIb from the garnet clinopyroxenite, although they have higher Mg-number $[Mg/(Mg + Fe^{2+})]$ and Cr_2O_3 concentrations (Table 2). Neoblastic clinopyroxenes, especially those of the fine-grained plagioclase-rich mylonitic bands, have low Al_2O_3 and Na_2O (Table 2, Fig. 6b). The Mg-numbers of both clinopyroxenes and orthopyroxenes (0·82–0·91 and 0·85–0·89, respectively) partially overlap those of the peridotites. Cr_2O_3 contents of clinopyroxenes range from 0·20 to 0·60 wt %. Amphibole is kaersutite with low K_2O (≤0·3 wt %) and moderate Cr_2O_3 (1·0–1·3 wt %). Spinel has Cr-number $[Cr/(Cr + Al)]$ and $Mg/(Mg + Fe^{2+})$ of 0·02–12 and 0·72–0·78, respectively. The green spinel in the symplectites and in the two-pyroxene assemblage has the lowest Cr-number. The highest Cr-numbers are observed in the greenish brown spinel from the olivine-bearing retrograde domains (Fig. 7). Primary and secondary olivines have high forsterite contents (Fo = 89–90 mol %).

Peridotites

The peridotitic olivine is Fo_{89}. Porphyroclastic spinel-facies clinopyroxene has high Al_2O_3, Na_2O and TiO_2 contents (6·7–8·6 wt %, 1·2–2·2 wt % and 0·6–1·0 wt %, respectively; see also Fig. 8a). Its Mg-number ranges from 0·89 to 0·92 and the Cr_2O_3 concentrations are 0·5–1·1 wt % (Fig. 8a, Table 3). The amounts of Al_2O_3 and Na_2O in porphyroclastic clinopyroxene decrease moderately from core to rim. The lowest Al_2O_3 and Na_2O contents (1·4–5·0 wt % and ≤0·6 wt %,

Table 2: Representative electron microprobe analyses of minerals in the websterite layers

Mineral	SiO_2	TiO_2	Al_2O_3	Cr_2O_3	FeO*	MnO	MgO	CaO	Na_2O	K_2O	Total	Mg-no.	Cr-no.	An
Sample BA3—Rio Strega														
Symplectite after garnet														
Grt (relic)	42·40	0·25	22·64	0·69	6·46	0·10	22·55	4·24	—	—	99·33	0·886	—	—
Opx	55·60	0·24	2·90	—	6·83	0·29	32·85	0·48	—	—	99·19	0·91	—	—
Spl	—	0·07	66·35	1·71	10·84	0·17	20·59	0·03	—	—	100·14	0·78	0·027	—
Pyroxene–spinel assemblage														
Cpx-p	49·93	0·41	10·59	0·33	3·22	0·11	15·65	19·12	0·78	—	100·14	0·897	—	—
Pl-e	52·81	—	28·72	—	0·20	—	—	12·34	5·00	—	99·07	—	—	42
Opx-p-c	54·23	0·04	4·89	0·22	7·56	0·10	31·57	0·92	—	—	99·54	0·886	—	—
Opx-p-r	54·76	0·00	3·62	0·24	7·65	0·35	32·17	0·69	—	—	99·47	0·894	—	—
Cpx-n	50·89	0·55	5·83	0·47	3·16	0·07	15·59	23·18	0·20	—	99·94	0·908	—	—
Opx-n	55·30	0·09	3·64	0·16	7·50	0·18	32·34	0·54	—	—	99·75	0·885	—	—
Spl-n	—	0·07	64·25	2·29	12·00	0·19	20·60	0·02	—	—	99·95	0·791	0·023	—
Sample AM353—Rio Strega														
Pyroxene–spinel assemblage														
Cpx-p	50·80	0·80	6·81	0·24	2·78	0·11	15·89	21·28	0·63	—	99·34	0·911	—	—
Opx-p	54·10	0·16	5·23	0·13	7·61	0·01	31·15	0·62	—	—	99·01	0·88	—	—
Spl	—	0·18	64·00	4·14	11·20	0·08	19·70	—	—	—	99·69	0·764	0·042	—
Olivine–plagioclase mylonitic band														
Ol	40·92	—	—	0·04	10·00	0·11	47·69	0·11	—	—	99·03	0·89	—	—
Pl	54·70	—	28·13	—	—	—	—	11·14	5·22	—	99·19	—	—	54
Cpx	53·34	0·25	2·00	0·33	2·49	—	17·99	22·94	—	—	99·34	0·82	—	—
Ks	42·30	5·25	12·40	1·15	4·46	0·04	15·60	12·00	3·35	0·10	96·65	0·86	—	—

*Total iron as Fe^{2+}.
Grt, garnet; Cpx, clinopyroxene; Opx, orthopyroxene; Spl, spinel; Pl, plagioclase; Ol, olivine; Ks, kaersutite. Mg-number = $Mg/(Mg + Fe^{2+})$; Cr-number = $Cr/(Cr + Al)$; An is anorthite mol %; p, porphyroclast; n, neoblast; c, core; r, rim; e, exsolution; —, not detected.

respectively) are shown by neoblastic plagioclase-facies clinopyroxene. Cr_2O_3 shows no significant variations between porphyroclastic and neoblastic clinopyroxenes (Fig. 8b).

Orthopyroxenes have Mg-numbers of 0·89–0·91. The cores of orthopyroxene porphyroclasts (Table 3) are Al_2O_3-rich (4·7–5·7 wt %) and contain variable amounts of CaO (0·6–1·4 wt %). The CaO and Al_2O_3 contents are lower in porphyroclast rims (0·5–0·7 wt % and 3·5–4·4 wt %, respectively). Orthopyroxene neoblasts have the lowest concentrations of Al_2O_3 and CaO (1·3–2·7 wt % and ~0·5 wt %, respectively). As a whole, the orthopyroxene analyses show a rough negative correlation between Al_2O_3 and CaO (Fig. 9).

Spinel shows (Fig. 7) variable Mg-number and Cr-number. This variability has been also found in the same sample and is probably related to the recrystallization under plagioclase-facies conditions. The lowest Cr-numbers are found in the cores of the rare porphyroclasts not rimmed by plagioclase, whereas increasing values occur towards the plagioclase coronas or in small relict crystals in plagioclase-bearing domains. TiO_2 contents in spinel are invariably lower than 0·25 wt %.

The brown amphibole porphyroclasts belonging to the spinel-facies assemblage range in composition from kaersutite to Ti-pargasite, according to the nomenclature of Leake *et al.* (1997). They have variable TiO_2 contents (3·4–5·3 wt %), even at the thin-section scale (Table 3, Fig. 10), and low to moderate K_2O concentrations (0·05–0·30 wt %).

Plagioclase is invariably anorthite-poor. The highest anorthite contents (48–56 mol %) were found in plagioclase coronas around spinel. The neoblastic grains in the mylonitic matrix have about 45 mol % anorthite and the plagioclase exsolution in the clinopyroxene porphyroclasts is albite-rich (An_{35}).

Pale green amphibole from the veins is Mg-hornblende, which spans a wide range of Al_2O_3 (4·3–10·4 wt %) and Na_2O (0·9–2·1 wt %) contents (Fig. 10).

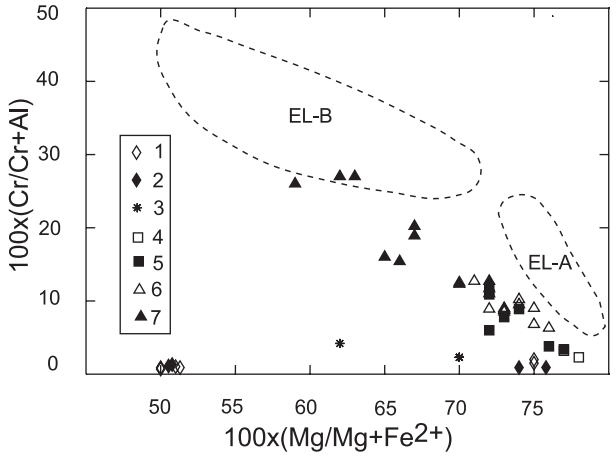

Fig. 7. 100 × [Cr/(Cr + Al)] vs 100 × [Mg/(Mg + Fe^{2+})] for spinels from pyroxenite layers and peridotites. 1–3, Garnet clinopyroxenites (1, Spl I from garnet-derived symplectites; 2, Spl II and III from pyroxene–spinel retrograde assemblage; 3, Spl IV from olivine-bearing retrograde assemblage); 4 and 5, websterites (4, spinel from pyroxene–spinel retrograde assemblage; 5, spinel from olivine-bearing retrograde assemblage); 6 and 7, peridotites (6, spinel porphyroclast cores; 7, spinel porphyroclast rims and relics in plagioclase-bearing domains). EL-A and EL-B, spinel porphyroclast cores and relics, respectively, in spinel-facies (Type A) and plagioclase-facies (Type B) peridotites from the southern External Liguride peridotites (Rampone *et al.*, 1995).

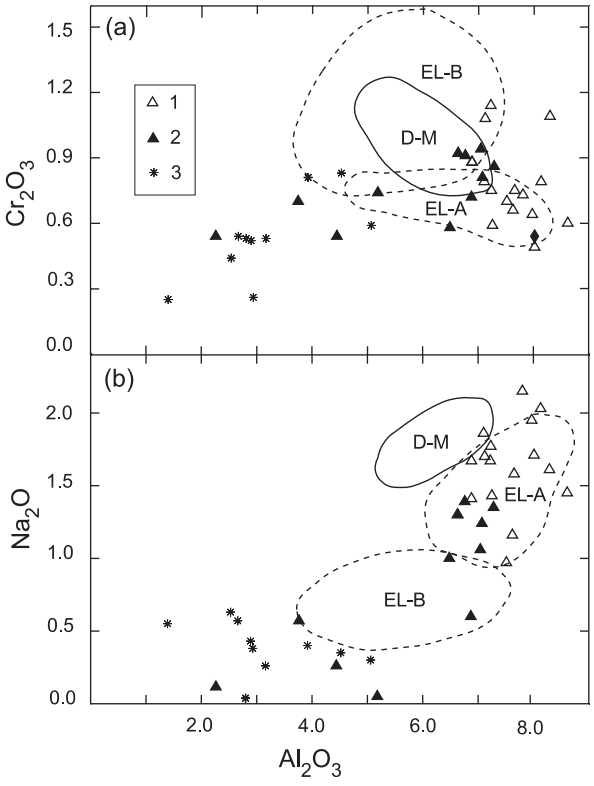

Fig. 8. Variation of Cr_2O_3 (a) and Na_2O (b) vs Al_2O_3 (wt %) for clinopyroxene from peridotites. 1, Porphyroclast cores; 2, porphyroclast rims; 3, neoblasts in plagioclase-facies assemblage. D-M, spinel-facies porphyroclasts cores from Malenco–Davos peridotites (Müntener *et al.*, 2004); EL-A and EL-B, porphyroclast cores and neoblasts, respectively, in spinel-facies (Type A) and plagioclase-facies (Type B) peridotites from the southern External Liguride peridotites (Rampone *et al.*, 1995).

Vein amphibole has TiO_2 concentrations between 0·14 and 0·75 wt %, and small amounts of Cl (≤0·18 wt %). Small prismatic tremolite crystals occur locally in the veins, probably as a later Mg-hornblende replacement (Table 4, Fig. 10). The colourless chlorite forming coronas around spinel (Table 4) is penninite.

The composition of serpentine (Table 4) varies in relation to the microstructural site of nucleation. Serpentine replacing olivine has low Al_2O_3 and Cr_2O_3 (<0·1 wt %), and relatively high NiO (0·15–0·38 wt %). On the other hand, fibrous serpentine after orthopyroxene has high Al_2O_3 (3·8–5·0 wt %) and Cr_2O_3 (0·17–0·44 wt %) contents, similar to those observed in the primary mineral, thus suggesting a relative immobility of these elements during serpentinization (Bonatti & Hamlyn, 1981; Agrinier *et al.*, 1988; Mével, 2003). FeO contents are variable in both types of serpentine pseudomorphs (4·9–7·8 wt %). The different veins belonging to the F_2 stage have low Al_2O_3 (1·2–2·8 wt %) and highly variable FeO contents (1·9–8·8 wt %). The lowest FeO values were observed for the serpentine with undulose extinction, which is probably older than the Fe-rich veins. Serpentine from the matrix of the F_3 jigsaw breccia has low to moderate Al_2O_3 (1·7–3·8 wt %), coupled with relatively high FeO. Non-pseudomorphic serpentine from both F_2 and F_3 stages commonly displays negligible Cr and Ni. Chlorine contents of the different serpentine types vary over a relatively wide range from 0·05 to 0·31 wt %, without a systematic relation with the nucleation site.

GEOTHERMOBAROMETRY

Conventional thermobarometry methods have been applied to minerals occurring in domains formed at different stages and distinguished on the basis of textural relations. Different cation exchange thermometers have been applied to both pyroxenites and enclosing peridotitic rocks to assess their thermal evolution, whereas pressure estimates have been obtained only for the garnet-bearing rocks (Table 5). To avoid the uncertainties related to Fe^{3+} recalculations from microprobe analyses, all iron in pyroxenes and garnet is assumed to be Fe^{2+}. The computed *P–T* estimates should, therefore, be considered as maximum values.

Pyroxenites

The occurrence of clinopyroxene inclusions (Cpx I) within garnets allows us to calculate the equilibration

Table 3: Representative electron microprobe analyses of minerals in the peridotites

	SiO_2	TiO_2	Al_2O_3	Cr_2O_3	FeO*	MnO	MgO	CaO	Na_2O	K_2O	Total	Mg-no.	Cr-no.	An
Sample AM324—Rio Strega														
Spinel-facies assemblage														
ol	40·11	—	—	0·04	10·23	0·21	49·54	0·01	—	—	100·14	0·900	—	—
cpx-p-c	51·22	0·67	7·80	0·73	2·93	0·13	13·66	20·76	2·15	—	100·05	0·968	—	—
cpx-p-r	50·70	0·85	6·76	0·91	2·83	0·02	14·16	21·35	1·39	—	98·97	0·916	—	—
opx-p-c	55·09	—	5·10	0·51	6·45	0·23	31·23	0·97	—	—	99·58	0·897		—
opx-p-r	54·91	0·21	3·87	0·29	6·60	0·30	32·31	0·55	—	—	99·04	0·897	—	—
spl-p	—	0·04	57·73	9·80	13·07	0·17	19·24	—	—	—	100·05	0·750	0·10	—
Ks-p	41·58	5·20	12·70	0·98	4·33	0·03	17·38	11·64	3·36	0·20	97·39	0·877	—	—
Ti-prg-p	41·24	3·81	13·92	0·82	4·34	0·01	18·29	11·20	3·27	0·20	97·08	0·889	—	—
Plagioclase-facies assemblage														
ol-n	41·50	0·04	—	—	10·68	0·14	48·13	—	—	—	100·49	0·890	—	—
cpx-n	52·69	0·67	2·53	0·44	2·89	0·20	16·27	22·63	0·63	—	98·95	0·921	—	—
opx-n	56·40	0·04	1·29	—	7·16	0·10	33·49	0·53	—	—	99·01	0·895	—	—
pl-n	58·10	—	25·74	—	0·17	—	0·07	10·51	6·55	—	101·14	—	—	47
spl (1)	—	0·04	41·80	21·90	21·45	0·36	14·70	—	—	—	100·25	0·622	0·26	
AM288b—Mt. Prinzera														
Spinel-facies assemblage														
ol	41·62	—	—	—	10·27	0·25	48·80	0·04	—	—	100·98	0·890	—	—
cpx-p-c	51·43	0·65	7·22	1·14	2·73		14·21	19·91	1·67	—	98·96	0·902	—	—
cpx-p-r	52·26	0·83	6·63	0·92	2·80	0·04	14·23	21·56	1·30	—	100·57	0·900	—	—
opx-p-c	54·45	0·14	5·22	0·30	7·15	0·24	32·02	1·13	0·06	—	100·71	0·902	—	—
opx-p-r	54·99	0·21	4·27	0·28	7·66	0·10	32·97	0·58	0·07	—	101·13	0·907	—	—
spl-p		0·17	58·74	8·68	12·35	0·16	18·81	—		—	99·20	0·730	—	—
Plagioclase-facies assemblage														
cpx-n	51·99	0·89	3·16	0·53	2·91		16·90	22·45	0·26	—	99·09	0·916	—	—
opx-n	55·46		1·88	0·25	7·18	0·12	34·90	0·50		—	100·29	0·929	—	—
spl-c (2)		0·24	55·82	11·64	13·76	0·33	17·85	0·40		—	100·04	0·700	0·09	—
spl-r (2)		0·22	49·00	18·55	15·43	0·45	16·45	0·14		—	100·24	0·670	0·12	—
pl (2)	55·41		27·62		0·14		0·13	10·14	5·91	—	99·34		0·20	48

*Total iron as Fe^{2+}.
Ol, olivine; Opx, orthopyroxene; Cpx, clinopyroxene; Spl, spinel; Pl, plagioclase; Ks, kaersutite; Ti-Prg, Ti-pargasite. Mg-number = $Mg/(Mg + Fe^{2+})$; Cr-number = $Cr/(Cr + Al)$; An is anorthite mol %; p, porphyroclast; n, neoblast; c, core; r, rim; —, not detected. (1), spinel relic in plagioclase-bearing mylonitic band; (2), Cr-rich spinel porphyroclast rimmed by plagioclase (3).

pressure and temperature of the early garnet clinopyroxenite assemblage. We have used the geobarometric method proposed by Simakov & Taylor (2000), based on the solubility of the Ca-Tschermaks component in clinopyroxene coexisting with garnet, which, recently, has been successfully applied to both diamond-bearing and diamond-free eclogite xenoliths (Peltonen *et al.*, 2002; Simakov, 2006). Temperature calculations are based on the application of the garnet–clinopyroxene Fe–Mg exchange reaction, according to the calibrations of Ellis & Green (1979), Krogh (1988), Ai (1994) and Krogh Ravna (2000). Pressures and temperatures were calculated iteratively using the clinopyroxene inclusions characterized by the highest Na_2O and Al_2O_3 contents (sample AM322, Table 5). Using the most recent calibration of the garnet–clinopyroxene geothermometer (Krogh Ravna, 2000), we obtained $T \sim 1100°C$ and $P \sim 2{\cdot}8$ GPa. The calibrations of Ellis & Green (1979), Krogh (1988) and Ai (1994) yield slightly higher temperature (and pressure) estimates. The high Al_2O_3 contents of Cpx I are consistent with the geothermobarometric evaluations. Experimental work has shown that clinopyroxenes with high proportions of Ca-Tschermaks molecule form at high-pressure

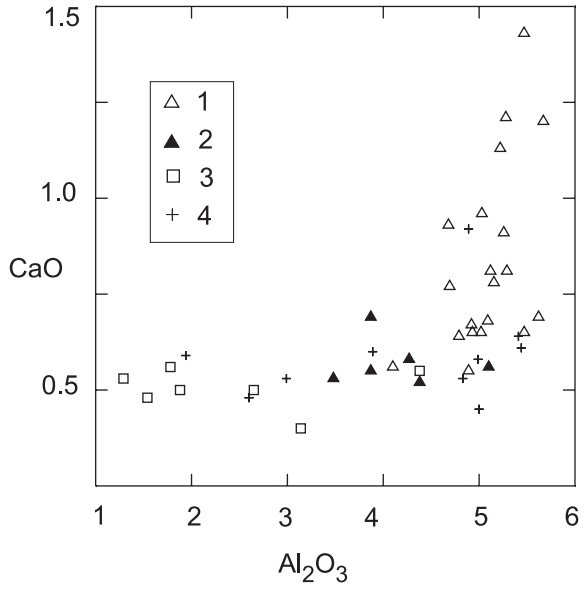

Fig. 9. Variation of CaO vs Al_2O_3 (wt %) for orthopyroxenes from spinel peridotites and olivine spinel websterites.

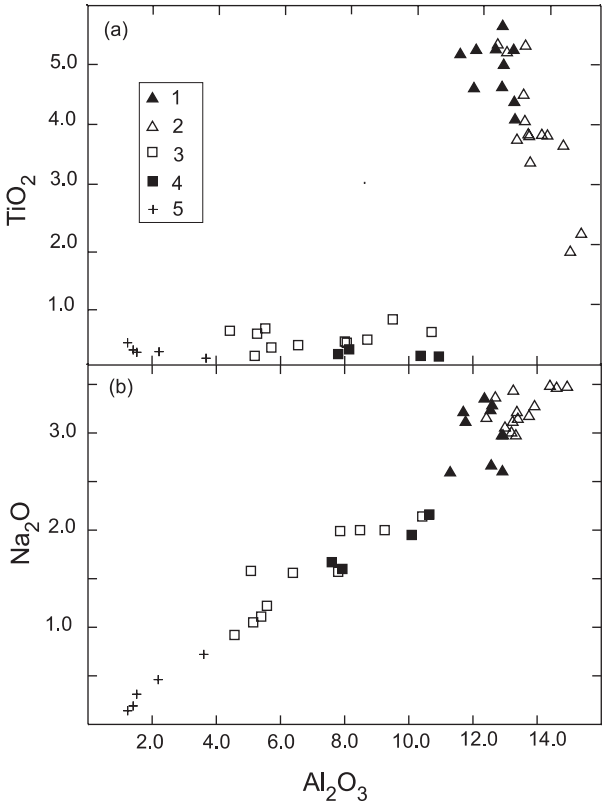

Fig. 10. Variation of TiO_2 (a) and Na_2O (b) vs Al_2O_3 (wt %) for amphiboles from pyroxenite layers and peridotites. 1 and 2, brown amphiboles (kaersutite and Ti-pargasite) from the spinel-facies assemblage of peridotites (1) and pyroxenites (2); 3 and 4, Mg-hornblende veins in peridotites (3) and pyroxenites (4); 5, retrograde tremolite in veins (3).

conditions (2·5–3·5 GPa) as segregations from basic melts (Thompson, 1974; Eggins, 1992; Johnson, 1998) and as residual phases after anhydrous partial melting of mafic rocks (Pertermann & Hirschmann, 2003; Yaxley & Brey, 2003). Jadeite contents in these magmatic or residual clinopyroxenes are typically low and comparable with those observed in the present study.

Pyroxene thermometry has been applied to the retrograde pyroxene–spinel-bearing assemblage of the garnet clinopyroxenites and websterites. The two-pyroxene geothermometer of Wells (1977) applied to small, undeformed clinopyroxene-orthopyroxene pairs (Cpx III–Opx II) of the garnet clinopyroxenites yields mean temperatures of ~960°C (Table 5). In addition, the neoblastic Cpx IV–Opx III pairs from a garnet clinopyroxenite layer characterized by dynamic recrystallization of pyroxenes + spinel gave $T = 920$°C. Similar temperature estimates were obtained for the clinopyroxene–orthopyroxene porphyroclasts and neoblasts from the websterites. We have also applied the Ca-in-Opx geothermometer of Brey & Kohler (1990) to the olivine-bearing websterites, which has yielded temperature estimates of ~950°C for the orthopyroxene porphyroclasts.

The coexistence of Ti-rich amphibole and plagioclase in the olivine-bearing domains of the retrogressed clinopyroxenites and websterites permits temperature to be estimated on the basis of the Holland & Blundy (1994) method. Temperature values of ~960°C have been obtained for both rock types.

Peridotites

Temperatures of the spinel- and plagioclase-facies equilibration in the peridotites have been estimated (Table 5) applying the Ca-in-Opx geothermometer (Brey & Kohler, 1990) and the Ca–Mg exchange geothermometers of Wells (1977) and Brey & Kohler (1990). The cores of spinel-facies orthopyroxene porphyroclasts yield $T_{\text{Ca-in-Opx}}$ estimates mainly ranging between 1000 and 1100°C, assuming $P = 1{\cdot}5$ GPa. Core to rim compositional variations in the orthopyroxene porphyroclasts reflect cooling of ~100–150°C. Two-pyroxene porphyroclast temperatures vary over a wide range, shifted to lower values (870–1040°C) than $T_{\text{Ca-in-Opx}}$ estimates based on the core compositions of orthopyroxene porphyroclasts. The lower estimates resulting from two-pyroxene geothermometers may be a consequence of pyroxene exsolution during slow cooling. The relatively low diffusivity of Ca in orthopyroxene compared with the Ca–Mg diffusivity in clinopyroxene (see Lenoir *et al.*, 2001) may have hampered complete re-equilibration of large orthopyroxene porphyroclasts during cooling. Temperature estimates for the plagioclase-facies equilibration range from 860 to 1030°C, on the basis of Cpx–Opx pairs.

Table 4: Representative electron microprobe analyses of the retrograde hydrous minerals

	Mineral	SiO_2	TiO_2	Al_2O_3	Cr_2O_3	FeO*	MnO	MgO	CaO	Na_2O	K_2O	NiO	Cl	Total
F_1 stage														
Pyroxenite														
1	Mg-Hbl	47·10	0·14	10·07	0·08	8·32	0·12	17·04	12·50	1·95	0·02	—	0·14	97·48
2	Chl	29·95	0·03	19·43	0·07	6·91	0·08	27·45	0·22	—	0·03	—	—	84·17
Peridotite														
3	Mg-Hbl	50·24	0·75	9·25	0·23	4·62	0·06	19·07	12·42	2·01	—	—	0·06	98·71
4	Mg-Hbl	54·07	0·14	5·08	0·15	3·38	0·03	22·50	11·42	1·58	0·03	—	0·03	98·41
5	Trm	56·90	0·21	2·19	0·41	2·40	0·01	22·70	12·28	0·46	—	—	—	97·56
6	Chl	36·50	—	15·08	0·08	4·17	0·14	31·40	—	—	0·16	—	—	87·53
F_2 stage														
Peridotite														
7	Srp	40·47	0·01	2·41	—	6·40	0·03	37·21	—	—	—	0·38	0·12	87·03
8	Srp	41·86	0·10	5·02	0·47	4·94		35·46	0·11	—	—	0·09	0·03	88·08
9	Srp	40·70	0·01	2·41	—	5·60	0·06	37·70	0·02		0·00		0·06	86·56
10	Srp	40·40	0·02	2·00	—	7·89	0·18	37·00	0·11	—	—	0·08	0·09	87·77
11	Srp	42·60	—	2·14	—	2·37	0·01	39·60	0·07	—	—	0·11	0·24	87·14
F_3 stage														
Peridotite														
12	Srp	42·00	—	3·67	—	6·62	0·24	35·00	—	—	—	0·16	0·14	87·83

*Total iron as Fe^{2+}.
1 and 2, Mg-hornblende + chlorite after pyroxene + plagioclase; 3 and 4, Mg-hornblende veins; 5, retrograde tremolite in veins; 6, chlorite corona around spinel; 7 and 8, serpentine pseudomorphs after olivine and orthopyroxene, respectively; 9 and 10, cross-cutting serpentine veins in partially serpentinized peridotite; 11, serpentine veins in foliated serpentinite; 12, serpentine matrix of the F_3 cataclasite.

Pressure evolution of the peridotites is difficult to constrain owing to the lack of appropriate geobarometers in garnet-absent systems. The pressure of the garnet–spinel transition in peridotitic systems is mainly controlled by the Cr content of the spinel (O'Neill, 1981; Webb & Wood, 1986; Klemme, 2004). In fertile compositions, characterized by spinel with Cr/(Cr + Al) <0·2, garnet is stabilized towards lower pressure values. A maximum pressure estimate for the spinel-facies equilibration can be determined on the basis of the formulation of Webb & Wood (1986). For this purpose we used the composition of spinel porphyroclast cores not rimmed by plagioclase and obtained pressure values of around 1·8 GPa. This pressure value is consistent with the *P–X* phase relations recently considered by Klemme (2004) for a simplified system $MgO–Cr_2O_3–Al_2O_3–SiO_2$.

Sm–Nd AND Lu–Hf GEOCHRONOLOGY

The summary of the isotopic results is presented in Table 6 and Fig. 11. Age calculations were performed using Isoplot® (Ludwig, 2003); age errors are given at the 95% confidence level.

A Sm–Nd isochron age is defined by whole-rock, plagioclase, clinopyroxene and two garnet fractions. The small scatter (MSWD = 0·26) together with the high $^{147}Sm/^{144}Nd$ values measured in garnets results in a well-constrained age of 186·0 ± 1·8 Ma (initial ε_{Nd} = +6·5). Remarkably, both garnet fractions resulted in identical (within error) isotopic ratios. The unusually high $^{147}Sm/^{144}Nd$ ratio of plagioclase is probably due to its metamorphic origin as a product of garnet + Cpx I breakdown, in a system characterized by an extreme LREE depletion (see also Tribuzio *et al.*, 2005). Although not all analysed minerals grew in equilibrium (e.g. garnet and plagioclase), the geothermometric investigations (Table 5) show that all analysed minerals crystallized significantly above 750–800°C, the closure temperature for the Sm–Nd system in garnet (Ganguly *et al.*, 1988; Van Orman *et al.*, 2002). Hence, the Sm–Nd isochron is interpreted as a cooling age, i.e. the garnet pyroxenite probably passed through the Sm–Nd blocking temperature at 186·0 ± 1·8 Ma.

Table 5: *P–T estimates for the different metamorphic assemblages in garnet-clinopyroxenites, websterites and peridotites*

	T(W) Cpx–Opx	*T*(BK) Cpx–Opx	*T*(BK) Ca(Opx)	*T*(HB) Pl–Amph	*P*(SK)–*T*(EG) Cpx–Grt	*P*(SK)–*T*(K) Cpx–Grt	*P*(SK)–*T*(Ai) Cpx–Grt	*P*(1)–*T*(KR) Cpx–Grt
Garnet clinopyroxenites								
Grt–Cpx I								
AM322					3·0–1130	3·0–1150	2·9–1140	2·8–1110
Cpx III + Opx II + Spl II + Pl								
AM322	960	960						
E181	998	1000						
AM288A	918	915						
Cpx IV + Opx III + Spl III + Pl								
AM288A	920	870						
Pl + Ol + Amph								
AM364				950				
AM333A				965				
Websterites								
Cpx (p) + Opx (p) + Spl ± Ol								
BA3 (W)	907	950						
BA4	930	982	910					
AM332	912	916						
AM353-1	946	961	966					
AM393	867	906	936					
Cpx (n) + Opx (n) + Spl (n)								
BA3-W	890	897						
Pl + Ol + Amph								
BA3-W				940				
Peridotites								
Spl facies (Ol+ Opx (p) + Cpx (p) + Spl)								
AM324	860	890	1020 (1100)					
BA3 (P)	865	885	980 (1050)					
AM372	932	973	1030 (1140)					
AM288B	945	969	1000 (1090)					
Pl facies (Ol + Opx (n) + Cpx (n) + Pl)								
AM324	885	885						
BA3-p	891	873						
AM372	932	973						
AM288B	1000	990						

Pressure (*P*) in GPa; temperature (*T*) in °C. References: W, Wells (1977); BK, Brey & Köhler (1990); HB, Holland & Blundy (1994); SK, Simakov & Taylor (2000); EG, Ellis & Green (1979); K88, Krogh (1988); Ai, Ai (1994); KR, Krogh Ravna (2000). Estimated error for the garnet–clinopyroxene geobarometer (Simakov & Taylor, 2000) is ±0·5 GPa, yielding an uncertainty of ±40°C on Grt–Cpx I *T* values. The reported values represent average estimates for each sample. (p), porphyroclast; (n), neoblast. (P) peridotite and (W) websterite band. *T* Ca(Opx) calculated for orthopyroxene cores at assumed P of 1.5 GPa; numbers in parentheses represent maximum *T* values obtained by this method for Ca-rich cores of large orthopyroxene porphyroclasts from peridotites. (For further explanation, see text.)

Lu–Hf dating of the same whole-rock and mineral fractions (excluding plagioclase) shows only ~0·06 spread in $^{176}Lu/^{177}Hf$ ratios, which does not give an age with high precision. The regression line with MSWD = 0·23 defines an age of 220 ± 13 Ma (initial ε_{Hf} = +4·5). Interpretation of the Lu–Hf age is more problematic, as little is known about the closure temperature for this system. It has been proposed that

Table 6: Sm–Nd and Lu–Hf data for the garnet-clinopyroxenite sample AM322

	Sm	Nd	$^{147}Sm/^{144}Nd$	$^{143}Nd/^{144}Nd$	εNd(i)	Lu (ppm)	Hf (ppm)	$^{176}Lu/^{177}Hf$	$^{176}Hf/^{177}Hf$	εHf(i)
WR	0·893	1·073	0·5032	0·513353 ± 8	+6·5	0·187	0·474	0·0558	0·283001 ± 6	+4·5
CPX	1·375	2·272	0·3658	0·513190 ± 7		0·108	0·736	0·0208	0·282858 ± 11	
GRT A	0·767	0·348	1·3339	0·514368 ± 15		0·220	0·359	0·0865	0·283124 ± 18	
GRT B	0·689	0·313	1·3335	0·514365 ± 11		0·196	0·327	0·0848	0·283124 ± 14	
PL	0·435	0·519	0·5069	0·513358 ± 9		–	–	–	–	

All errors are 2SE and relate to the last significant digits, except for age errors, which are 95% confidence level. Decay constant $\lambda^{176}Lu = 1{\cdot}865 \times 10^{-11}$ year^{-1} (Dalmasso *et al.*, 1992; Scherer *et al.*, 2001). Values used for εHf(*t*) calculations: $^{176}Hf/^{177}Hf_{CHUR(0)} = 0{\cdot}282772$ and $^{176}Lu/^{177}Hf_{CHUR(0)} = 0{\cdot}0332$ (Blichert-Toft & Albarede 1997). Values used for εNd(*t*) calculations: $^{143}Nd/^{144}Nd_{CHUR(0)} = 0{\cdot}512647$ and $^{147}Sm/^{144}Nd_{CHUR(0)} = 0{\cdot}1966$ (Jacobsen & Wasserburg 1980).

the closure temperature for Lu–Hf in garnet is equal to, or slightly higher (~100°C) than for Sm–Nd (Scherer *et al.*, 2001). Although few coupled Lu–Hf and Sm–Nd age determinations have been carried out on mantle garnet-bearing rocks, the available data corroborate this interpretation. Lu–Hf cooling ages older than Sm–Nd ages have been reported for garnet pyroxenite layers from Beni-Bousera (Blichert-Toft *et al.*, 1999; Pearson & Nowell, 2004) and for a garnet pyroxenite sample in a Mirdita (Albania) ophiolite (Blichert-Toft *et al.*, 1999), in agreement with this notion. In particular, the large difference between the Lu–Hf and Sm–Nd mineral isochron ages (203 ± 3·4 Ma and 166 ± 2 Ma, respectively) obtained for the Mirdita ophiolite sample is similar to that found for the External Liguride pyroxenite in this study. In addition, recent work on eclogite xenoliths in kimberlites (Bedini *et al.*, 2004) yielded Lu–Hf clinopyroxene–garnet ages generally older than the corresponding Sm–Nd ages. This suggests that radiogenic Hf diffuses out of garnet more slowly than radiogenic Nd, giving further support to the notion that Tc(Lu–Hf) ≥ Tc(Sm–Nd). Because the estimated temperature for garnet equilibration in the studied rock is ~1100°C (i.e. above any reasonable closure temperature for the Lu–Hf system; see also Bedini *et al.*, 2004), it seems plausible to interpret the Lu–Hf age in terms of cooling.

DISCUSSION

Decompression-related evolution of pyroxenite layers

Textural observations indicate that the retrograde transformations within the garnet clinopyroxenites started with the breakdown of the garnet + Al-rich clinopyroxene assemblage to a garnet-free two-pyroxene + spinel + plagioclase assemblage. The bulk mineralogical composition (Opx + Spl + Pl + Cpx) of the coronas around garnet in the garnet clinopyroxenites indicates that breakdown of garnet and clinopyroxene was coupled with element diffusion across the boundary between the two phases, suggesting a general reaction

$$\text{Grt} + \text{CpxI} = \text{OpxII} + \text{SplI} + \text{Pl} + \text{CpxIIa}.$$

The corona mineral zonation, characterized by formation of Opx II + Spl I + Pl in an inner zone and of the same phases along with secondary clinopyroxene (Cpx IIa) adjacent to Cpx I, probably developed as a result of chemical potential gradients and consequent element diffusion throughout the corona. Similar microtextures have been observed for other garnet pyroxenites (Obata, 1994) and peridotites (Godard & Martin, 2000) exhumed from great depths. The breakdown of primary clinopyroxene to a secondary clinopyroxene (Cpx IIb) with lower Ca-Tschermaks and jadeite contents + plagioclase (Pl Ib) is commonly observed for clinopyroxenes from retrogressed eclogites (e.g. Boland & Van Roermund, 1983; Joanny *et al.*, 1991).

In the Mg-rich garnet clinopyroxenites and websterites, the breakdown products of garnet include spinel and secondary orthopyroxene and clinopyroxene, in the absence of plagioclase. The relatively high Na contents of both secondary clinopyroxene and bulk symplectite (Tables 1 and 2) indicate that the symplectites are not simply the result of garnet decomposition, requiring the involvement of an earlier Na-bearing phase in the reaction, probably a primary clinopyroxene that has not been preserved. In addition, the bulk symplectite compositions have excess Mg, suggesting a contribution from primary olivine (Morishita & Arai, 2003) or orthopyroxene. The following reaction is therefore proposed:

$$\text{Grt} + \text{CpxI} + \text{Ol/OpxI} = \text{OpxII} + \text{SplI} + \text{CpxIIa}.$$

In both garnet clinopyroxenites and websterites, coarsening and recrystallization of the breakdown products

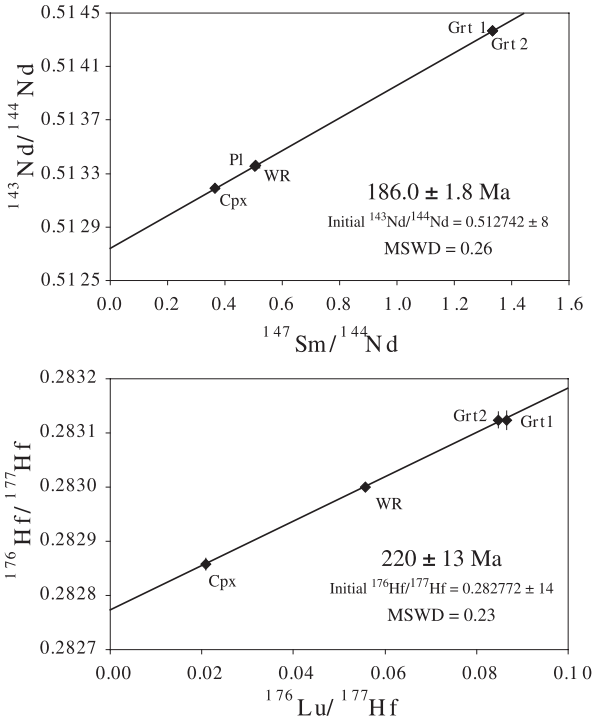

Fig. 11. Sm–Nd and Lu–Hf isochron diagrams for the garnet pyroxenite sample AM322. Cpx, clinopyroxene; Grt, garnet; Pl, plagioclase; WR, whole-rock.

from the primary garnet-bearing assemblage led to partial textural re-equilibration and the formation of allotriomorphic or granoblastic textures. Subsequent deformation and dynamic recrystallization of the newly formed assemblage is shown by sheared pyroxene porphyroclasts mantled by fine-grained grained two-pyroxene + spinel ± plagioclase aggregates. Progressive Na_2O and Al_2O_3 decrease in the different generations of retrograde clinopyroxenes (Fig. 6), corresponding to decreasing amounts of jadeite and Ca-Tschermaks substitution, is consistent with both decompression and cooling during the retrograde evolution (White, 1964; Gasparik, 1984). This is also consistent with the remarkable grain-size decrease towards the inner portion of the coronas between garnet and primary clinopyroxene (e.g. Messiga & Bettini, 1990). Geothermometry results for the pyroxenites actually show that the evolution from garnet–to pyroxene–spinel assemblage involved significant cooling (Table 5).

The garnet stability field for mafic to ultramafic systems is known to expand with decreasing whole-rock Mg and Cr, and increasing Al (O'Neill, 1981; Nickel, 1986; O'Hara *et al.*, 1971; Klemme, 2004), so that garnet may be stable at lower pressure in pyroxenite than in peridotite. The pressure of garnet breakdown can be roughly constrained considering the experimental curves obtained for mafic systems (e.g. Irving, 1974; Adam *et al.*, 1992). The pressure of garnet (+ Cpx I ± Ol ± Opx I) breakdown to Cpx II + Opx II + Spl I ± Pl in garnet clinopyroxenites and websterites approximately lies in the range 1·2–1·5 GPa, assuming $T = 1000°C$. This decompression stage was accompanied by significant cooling (Table 5).

A later decompression stage is recorded by the local formation of olivine + plagioclase after two-pyroxenes + spinel in different microstructural sites. Similar decompression-related subsolidus formation of olivine + plagioclase coronas has been reported for pyroxenite layers within other peridotite massifs (e.g. Van der Wal & Vissers, 1996) and within the peridotites drilled along the western Iberian margin (Cornen *et al.*, 1996). The increase of Cr-number commonly observed in the spinel from the olivine-bearing domains (in the websterites) may be accounted for by the breakdown of relatively Cr-rich clinopyroxene according to the reaction Cpx + Opx + Al-Spl = Ol + Pl + Cr-Spl. The olivine + plagioclase formation is commonly associated with the involvement of the pyroxenite layers in the mylonitic deformation that affected the host peridotite under plagioclase-facies conditions. In garnet clinopyroxenites, in addition, olivine locally developed as a late breakdown product of garnet relics, together with plagioclase and spinel. The reaction Grt = Ol + Pl + Spl is not frequently observed in garnet pyroxenites or eclogites, but has been reported as a LP–HT retrograde stage in retrogressed eclogites from the Bohemian Massif (O'Brien, 1997). The conversion of the pyroxene + spinel to olivine + plagioclase may be approximately constrained at a pressure of 0·7–0·8 GPa (Green & Ringwood, 1967; Irving, 1974; Adam *et al.*, 1992).

The temperatures calculated for the two-pyroxene porphyroclastic and neoblastic garnet- and olivine-free assemblages of both garnet clinopyroxenites and garnet websterites overlap significantly and are not distinguishable from those of the olivine-bearing stage inferred from amphibole in equilibrium with plagioclase (Table 5). This indicates that the late stage of the decompression path was nearly isothermal.

Decompression-related evolution of the peridotites and origin of the plagioclase

No mineralogical evidence has been preserved for an early garnet-bearing assemblage in the peridotites of the present study. However, the pressure estimate of 2·8 GPa for the garnet clinopyroxenite assemblage [even considering the large uncertainty reported for the Simakov & Taylor (2000) geobarometer], suggests that the investigated mantle section underwent a previous stage of equilibration under garnet-facies conditions. The relatively low pressure required for the

spinel–garnet transition in a peridotitic system characterized by Cr-poor spinel further supports this view. The early occurrence of garnet was also hypothesized by Rampone *et al.* (1995) for the southernmost External Liguride peridotite bodies on the basis of clinopyroxene trace element compositions. In addition, the presence of rounded orthopyroxene–spinel clusters indicating a former garnet-bearing precursor has been reported for other subcontinental peridotite bodies of the Alpine–Apennine system exhumed during the same geodynamic event, i.e. Erro–Tobbio (Ligurian Alps, Hoogerduijn Strating *et al.*, 1993) and Lanzo (Western Alps, Piccardo *et al.*, 2004*a*). In the External Liguride peridotites, therefore, the original garnet-bearing assemblage was probably erased by re-equilibration under spinel-facies conditions.

The spinel peridotite assemblage in the studied peridotites is preserved in relict domains within the plagioclase mylonite. These domains display a porphyroclastic texture testifying to the development of a former spinel-facies tectonite. The $T_{\text{Ca-in-Opx}}$ registered by the cores of some of the orthopyroxene porphyroclasts, consistent with those obtained for the garnet–pyroxene assemblage of the pyroxenite layers, may preserve a record of the former garnet-facies equilibration. On the other hand, two-pyroxene and plagioclase–amphibole geothermometry indicates that the spinel- and plagioclase-facies recrystallizations occurred under similar temperature ranges; that is, the related decompression did not involve significant cooling.

The thermal history of the investigated mantle section, the fertile nature of the peridotites and the preservation of basic pyroxenite layers, which are characterized by lower melting temperatures than the host peridotite (Hirschmann & Stolper, 1996), rule out partial melting as an origin for the plagioclase. Plagioclase growth in the External Liguride peridotites has been ascribed to subsolidus decompression in Middle to Late Jurassic times (Rampone *et al.*, 1993, 1995). Recent studies, however, have provided new textural and geochemical evidence indicating that some of the External Liguride peridotites experienced extensive melt–rock reaction, impregnation and heating by ascending asthenospheric melts during the opening of the Ligurian Tethys (Müntener & Piccardo, 2003; Müntener *et al.*, 2004). However, the peridotites of the present study lack typical reaction or impregnation microtextures, even in the portions unaffected by the plagioclase-facies mylonitic deformation. In addition, chemical features indicating infiltration and reaction with basaltic melts (e.g. Ti enrichment of spinel and/or clinopyroxene) are lacking.

The studied peridotites have remarkably similar parageneses (i.e. occurrence of Na–Al-rich clinopyroxene porphyroclasts coexisting with Cr–Ti-poor spinels) to other Ligurian Tethys peridotites interpreted as old lithospheric mantle domains that had escaped impregnation processes (Rampone *et al.*, 1995; Müntener *et al.*, 2004; Piccardo *et al.*, 2004*a*). In addition, there is no geothermometric indication of local heating to near-asthenospheric conditions, as recorded, for example, in other mantle bodies from the External Liguride domain (Piccardo *et al.*, 2004*a*), which could result from melt infiltration. We conclude that plagioclase formed at subsolidus conditions during exhumation of this mantle section. Such a process is also recorded by clinopyroxene compositions, which show a decrease of Al_2O_3 and Na_2O from porphyroclast cores to rims, and to neoblasts (Fig. 8a; see also Rampone *et al.*, 1993, 1995). The similar Al_2O_3 decrease between orthopyroxene porphyroclasts and neoblasts (Fig. 9) is consistent with the inferred process of plagioclase-facies re-equilibration. The lack of a concomitant Cr_2O_3 increase in clinopyroxene and orthopyroxene, as expected in spinel-free recrystallized assemblages (Rampone *et al.*, 1993), can probably be accounted for by Cr redistribution in the relict spinel, which is significantly enriched in Cr with respect to the porphyroclastic spinel (Table 3).

Maximum pressure estimates for the plagioclase-facies equilibration have been obtained using the reaction orthopyroxene + clinopyroxene + spinel = olivine + plagioclase. The intersection between the temperature calculated for the neoblastic Cpx–Opx pairs in the plagioclase-bearing assemblage and the curve obtained by interpolating the curves of Newman *et al.* (1998) for the albite-rich plagioclase compositions of the analysed peridotites constrain the pressure of the spinel to plagioclase transition at 0·8–0·9 GPa.

The fine-grained polyphase matrix of the plagioclase mylonites, characterized by grain boundary alignment parallel to the mylonitic foliation, is analogous to that described in other anhydrous plagioclase mylonites, where grain-size sensitive creep (including diffusion creep and grain boundary sliding) acts as the dominant deformation mechanism (e.g. Newman *et al.*, 1998; Furusho & Kanagawa, 1999; Dijkstra *et al.*, 2002). The plagioclase mylonite assemblage locally includes trace amounts of Ti-rich amphibole, suggesting that deformation took place in an H_2O-deficient environment. Notably, an external fluid input is not required at this stage, as the small amphibole amounts found in the plagioclase domains may form at the expense of the Ti-rich amphibole occurring in the spinel-bearing assemblage. The formation of 100-m-scale shear zones made up of plagioclase mylonites is consistent with the concept that subsolidus plagioclase formation under decompression, possibly associated with grain-size reduction, may lead to reduction of the lithospheric mantle strength, promoting strain localization and development of large shear zones ('reaction-enhanced ductility'; see Newman *et al.*, 1998; Furusho &

Kanagawa, 1999; Handy & Stünitz, 2002; de Ronde *et al.*, 2004).

P–T conditions of retrograde hydration stages

The anhydrous high-temperature ductile evolution is overprinted by episodes of deformation (F_1 to F_3 stages) occurring in a brittle regime. In particular, the formation of Mg-hornblende ± chlorite in veins and as pseudomorphs after clinopyoxene and brown amphibole in both pyroxenites and peridotites marks the onset of hydration of the studied mantle section. Unfortunately, no clear textural evidence of an equilibrium assemblage (e.g. coexistence of hornblende + chlorite with olivine and a spinel phase in peridotites) is preserved, thus precluding the evaluation of accurate *P–T* conditions for the onset of hydration. Nevertheless, the early formation of an aluminous amphibole instead of tremolite indicates amphibolite-facies conditions (Evans, 1982), thus yielding a conservative minimum temperature of ~500°C for the early hydration event. An upper temperature limit is provided by chlorite stability in ultramafic systems at low-pressure conditions (~700°C, Schmidt & Poli, 1998; Ulmer & Trommsdorff, 1999).

Pressure estimates for the amphibolite-facies event are provided by the absence of epidote in the Mg-hornblende + chlorite assemblage within mafic pyroxenite layers, which indicates $P \leq 0{\cdot}3$ GPa (Liou *et al.*, 1974; Apted & Liou, 1983). The appreciable Cl contents of the Mg-hornblende imply an external fluid source whose origin is difficult to constrain. Hornblende veining was observed in mantle rocks from the western Iberia margin and attributed to interaction with seawater-derived fluids (Kimball & Evans, 1988). Alternatively, continental crust derivation of Cl-rich fluids migrating from thinned overlying crust could be hypothesized, as proposed by Muntener *et al.* (2000) for the hydration of the lower crustal–upper mantle sequence of Val Malenco (Central Alps).

The amphibole compositional variations, i.e. decreasing amount of edenite and Ti-tschermakite substitution (Fig. 10), indicate a metamorphic evolution characterized by decreasing temperature conditions. The *P–T* conditions of the subsequent retrograde evolution during the F_2 stage, dominated by intense brittle fracturing and serpentinization, are difficult to constrain. No definitive consensus on lizardite thermal stability exists. It should form at low temperature (<300°C) during low-pressure retrograde metamorphism (Evans *et al.*, 1976; O'Hanley, 1996; Evans, 2004), but departure from the ideal formula by incorporation of Fe and Al enlarges its thermal stability up to 400–500°C (e.g. Caruso & Chernosky, 1979; O'Hanley *et al.*, 1989). However, it has been experimentally shown that under relatively high-temperature conditions ($T = 400$°C) orthopyroxene and clinopyroxene are altered into talc and tremolite, respectively, in ultramafic systems, whereas olivine remains stable (Allen & Seyfried, 2003). The absence of talc pseudomorphs after orthopyroxene in the studied peridotites suggests that the main hydration event started at low-grade conditions, unless talc was later replaced by serpentine.

Several features of the jigsaw breccia formed during the F_3 stage, such as the extremely wide range of clast size, the matrix made of comminuted serpentinite fragments and the absence of significant clast displacement, indicate a tectonic origin. Similar cataclastic rocks have been observed in the upper levels of the mantle exhumed along the western Iberia margin (Comas *et al.*, 1996). The jigsaw-puzzle pattern of fractures indicates expansion in all directions and is considered diagnostic of fluid-induced, fault-related implosion brecciation (Sibson, 1987). The occurrence of polyphase cracking and veining suggests a complex interplay of extensional stresses leading to intermittent rupturing of the partially serpentinized peridotite, fluid infiltration and precipitation of new phases. In particular, the formation of spherulitic serpentine ± spheroidal calcite in the cataclasite matrix requires rapid growth from nucleation sites in a hydrothermal fluid (Sibson, 1987; Skelton & Valley, 2000).

The precipitation of Cl-bearing serpentine + sulphides + calcite in the cataclasite matrix indicates the involvement of Cl-, CO_2- and S-bearing fluids. In particular, the pyrite + millerite + calcite assemblage indicates high f_{S_2} conditions and high water:rock ratios (Frost, 1985; Palandri & Reed, 2004); the late calcite + pyrite veins, which crosscut all the earlier brittle structures, could be ascribed to cold seawater-related alteration ($T < 50$°C; Hopkinson *et al.*, 2004). Textural and mineral analogies between the F_3 cataclasites and the uppermost levels of the serpentinized mantle exhumed along the western Iberia margin (Comas *et al.*, 1996; Alt & Shanks, 1998) support the notion that the investigated mantle section was emplaced at shallow levels, in proximity to the ocean floor.

Pressure–temperature–time evolution of the External Liguride mantle section

Combining petrographic and mineral chemistry data with thermobarometric estimates for both pyroxenites and peridotites, the following *P–T* evolution (Fig. 12) has been reconstructed for the External Liguride mantle section: (1) equilibration occurred under garnet-facies conditions ($P \sim 2{\cdot}8$ GPa, $T \sim 1100$°C), compatible with a relatively hot subcontinental geotherm (Fig. 12), which rules out the possibility that this early high-pressure stage was related to involvement of these mantle rocks in the

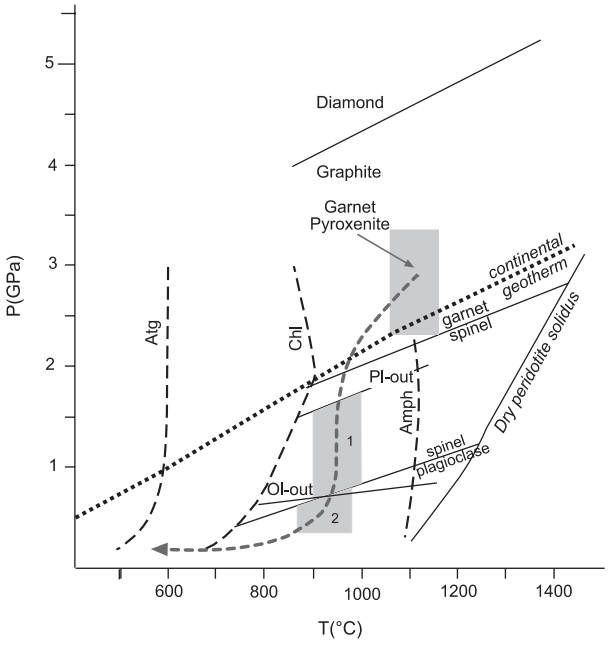

Fig. 12. Schematic *P–T* diagram for the studied mantle section. Diamond–graphite boundary after Kennedy & Kennedy (1976); pargasitic amphibole stability field in pyrolite composition from Niida & Green (1999); the dotted curve is a mantle geotherm for tectonically active continental areas (Röhm *et al.*, 2000); plagioclase- and olivine-out curves for mafic systems after Green & Ringwood (1967); chlorite and serpentine (Atg) stability fields after Ulmer & Tromsdorff (1999). Shaded boxes (1) and (2) are the *P–T* intervals for spinel- and plagioclase-facies equilibration, respectively.

Variscan subduction event, in contrast to other mantle bodies now exposed in the Eastern Alps (Tumiati *et al.*, 2003); (2) an early decompression stage, shown by garnet breakdown in the pyroxenites and associated with the formation of the spinel tectonite fabric in the peridotites, occurred under moderately decreasing temperature ($P \leq 1{\cdot}8$ GPa, $T \sim 950$°C); (3) further, nearly isothermal, decompression to $P \leq 0{\cdot}8$ GPa led to the development of plagioclase-bearing peridotite mylonites and growth of the olivine + plagioclase association in the pyroxenites; (4) inception of hydration occurred under amphibolite (Mg-hornblende + chlorite)-facies conditions at $P \leq 0{\cdot}3$ GPa and $T = 500$–700°C, coupled with brittle fracturing; (5) shallow-level polyphase brittle deformation occurred, associated with peridotite serpentinization, which culminated in sea-floor exposure.

As the closure temperature of the Sm–Nd system is higher than the temperature estimated for Mg-hornblende vein formation, the Sm–Nd isochron age of 186·0 ± 1·5 Ma represents a maximum time estimate for the onset of mantle hydration. In addition, the Lu–Hf isochron indicates that the mantle section cooled below 750–900°C (i.e. the inferred closure temperature of the Lu–Hf system) at 220 ± 13 Ma, which may be a minimum age for the development of plagioclase-facies mylonites. The ages obtained by the Sm–Nd and Lu–Hf methods thus record a retrograde history of slow cooling (≤5°C/Ma) in the plagioclase stability field between the Late Triassic and the Early Jurassic. The retrograde evolution from plagioclase- to amphibolite-facies conditions was probably associated with the intrusion of syn-rift MOR-type gabbros in other sectors of the External Liguride mantle section, which have given Sm–Nd clinopyroxene–plagioclase–whole-rock isochron ages of 179 ± 9 Ma (Tribuzio *et al.*, 2004).

Two peridotites from the southernmost Mt. Nero body of the External Liguride units yielded Sm–Nd clinopyroxene–plagioclase isochron ages of 163 ± 20 Ma and 165 ± 20 Ma (Rampone *et al.*, 1995). These ages were interpreted to date the exhumation of the External Liguride mantle section to plagioclase-facies conditions, thus contrasting with the Lu–Hf age reported in this study, unless the mantle bodies from the External Liguride domain record diachronous exhumation. The Mt. Nero mantle body retains a fertile geochemical signature but is pyroxenite-poor, characterized by the occurrence of impregnated plagioclase-rich peridotites and locally intruded by basaltic dykes and small gabbroic bodies (Terranova & Zanzucchi, 1984; Piccardo *et al.*, 2004*b*; Poggi *et al.*, 2005). In addition, the Mt. Nero peridotites display typical MORB-like Nd and Sr isotope compositions (Rampone *et al.*, 1995). It seems plausible, therefore, that the age reported by Rampone *et al.* (1995) records the effects on the previously exhumed lithospheric mantle of MORB–rock reaction and MORB impregnation associated with plagioclase formation (see also Müntener & Piccardo, 2003).

In the External Liguride units, lower crustal granulites derived from gabbroic protoliths of Late Palaeozoic age yielded an $^{40}Ar/^{39}Ar$ amphibole cooling age of 228 ± 2 Ma (Meli *et al.*, 1996). This radiometric date is within error of the Lu–Hf cooling age obtained from the garnet pyroxenites in the present study. When the mantle section was under temperature conditions of 750–900°C, therefore, the gabbro-derived granulites cooled below a temperature of about 500°C (see also Marroni *et al.*, 1998). The subsequent sequence of low-temperature brittle deformations recorded by the lower crustal rocks (see also Montanini, 1997) was related to their exhumation in conjunction with the rifting event that led to oceanization in the Middle Jurassic.

Timing of the high-temperature decompression

The relationships between high-temperature structures and rifting processes in the mantle exhumed along modern and fossil non-volcanic margins are puzzling (e.g. Whitmarsh *et al.*, 2001; Manatschal, 2004). In the case of the External Liguride mantle section, constraints

on the timing of high-temperature exhumation from garnet- to plagioclase-facies conditions are provided by new geochronological, petrological and regional geological data.

The Mesozoic rifting that led to the opening of the Ligurian Tethys was preceded by Late Palaeozoic (Late Carboniferous to Early Permian) extensional processes associated with extensive tholeiitic magmatism (Voshage *et al.*, 1990; Tribuzio *et al.*, 1999; Hermann *et al.*, 2001; Montanini & Tribuzio, 2001). The Late Palaeozoic extension was related to asthenospheric upwelling, possibly following delamination of a lithospheric root (Schott & Schmeling, 1998; Arnold *et al.*, 2001) at the end of the Variscan orogeny. Whether the Late Palaeozoic extension and Mesozoic rifting reflected a continuous evolution that led to continental rifting (Piccardo *et al.*, 1990; Lardeaux & Spalla, 1991; Dal Piaz, 1993) or were related to independent geodynamic processes (Handy & Zingg, 1991; Müntener *et al.*, 2000; Müntener & Hermann, 2001) is still a matter of debate.

In this tectonic framework, the exhumation of the External Liguride mantle section from garnet- to plagioclase-facies conditions may have occurred in a unique stage starting in the Late Palaeozoic to Triassic, similar to that proposed by Vissers *et al.* (1991) for the the Ligurian Alps peridotites. However, the inferred change of slope in the decompressional P–T path (Fig. 12) is difficult to reconcile with this evolution, suggesting that exhumation may have been accomplished through two distinct decompression stages, probably related to separate geodynamic events.

Two main scenarios may thus be envisaged for the timing of the high-temperature decompression recognized for the External Liguride mantle section. In the first, the nearly isothermal decompression from spinel- to plagioclase-facies conditions occurred in relation to Late Palaeozoic lithospheric thinning, and the previous exhumation from the garnet to spinel stability field was related to an ancient geodynamic event. Such a scenario is supported by the comparison with the mantle sequence from Erro Tobbio (Western Alps), which records a similar high-temperature decompression (Vissers *et al.*, 1991; Hoogerduijn Strating *et al.*, 1993). On the basis of Sm–Nd clinopyroxene–plagioclase–whole-rock isochrons yielding ages of 313 ± 13 Ma and 273 ± 16 Ma, Rampone *et al.* (2005) recently ascribed the decompression from spinel- to plagioclase-facies conditions of the Erro-Tobbio peridotite to Late Palaeozoic lithospheric extension. The second scenario implies that the decompression from garnet- to spinel-facies conditions was related to the Late Palaeozoic evolution, and that the subsequent exhumation associated with plagioclase-facies shear zone formation was due to the onset of Mesozoic rifting (i.e. it occurred in Triassic times).

In the Northern Apennines, evidence for Middle Triassic rifting phases is provided by the lower crustal granulites from the External Liguride units (Marroni *et al.*, 1998; see preceding section) and by the occurrence of an extensional basin sequence consisting of Middle Triassic marine deposits (Martini *et al.*, 1986) associated with alkali basaltic lava flows (Ricci & Serri, 1975). Evidence for rift-related Middle Triassic faults (e.g. Bertotti *et al.*, 1993, 1999) and coeval involvement of mantle-derived melts with alkaline affinity (e.g. Stähle *et al.*, 1990, 2001) is also reported for the South Alpine domain of the Western Alps. In addition, preliminary geochemical and geochronological investigations of the Finero gabbroic complex (South Alpine domain of Western Alps) have shown a MOR-type affinity for the parental melts and an intrusion age of about 230 Ma, thus testifying to asthenospheric ascent in Middle to Late Triassic times (Peressini *et al.*, 2004).

The comparison with the P–T–t path of the fosssil mantle–lower crust section cropping out at Malenco, in the central Alps (Müntener *et al.*, 2000; Villa *et al.*, 2000; Müntener & Hermann, 2001), supports the idea that the near-isothermal decompression recorded by the External Liguride mantle section was of Triassic age. The spinel-facies mantle peridotites from Malenco equilibrated at the base of the continental crust ($P = 1{\cdot}0$–$1{\cdot}2$ GPa) in Late Palaeozoic times, at relatively low-temperature conditions ($T \sim 800$°C). The subsequent evolution of the Malenco peridotites was characterized by a Late Palaeozoic isobaric cooling stage that was followed by near-isothermal decompression (from 0·8 to 0·4 GPa, at ~550°C) associated with hydration and development of olivine + tremolite + chlorite mylonites (Müntener *et al.*, 2000; Villa *et al.*, 2000; Müntener & Hermann, 2001). The near-isothermal decompression started at about 225 Ma, on the basis of $^{40}Ar/^{39}Ar$ amphibole age determinations, and has been attributed to the onset of the rifting event that led to continental break-up. The $^{40}Ar/^{39}Ar$ amphibole age of the Malenco section is close to the time at which the External Liguride mantle passed through the Lu–Hf blocking temperature (750–900°C), under plagioclase-facies conditions. The Malenco and External Liguride mantle sections were, therefore, at different thermal conditions in Middle to Late Triassic times. The higher temperature recorded by the External Liguride mantle section may reflect its rapid uplift from deeper, spinel-facies mantle levels. If the spinel- to plagioclase-facies decompression was of Late Palaeozoic age, as envisaged for the first scenario, the External Liguride mantle section must have remained in the plagioclase stability field for 90–130 Myr. Maintaining these high-temperature–low-pressure conditions for such a long time span is difficult to reconcile with a realistic geodynamic model.

Although the new geochronological data are not conclusive, we propose a Middle to Late Triassic age for the near-isothermal spinel- to plagioclase-facies decompression recorded by the External Liguride mantle section. This decompression probably occured in conjunction with the onset of the rifting that led to the opening of the Ligurian Tethys in the Middle Jurassic. The subsequent slow cooling in the plagioclase stability field, as indicated by Sm–Nd and Lu–Hf mineral isochrons for the garnet pyroxenites, is consistent with a rifting situation in which conductive heat loss was partially counteracted by the underlying ascending asthenosphere. Such asthenospheric ascent during the Late Triassic to Early Jurassic evolution could be related to the melt impregnation processes recorded by the southernmost mantle bodies of the External Liguride units (Müntener & Piccardo, 2003). The age of such melt–peridotite interactions is not known, but could precede the intrusion of the syn-rift gabbros, which represent an advanced stage of the process of upward migration of asthenospheric melts (Piccardo *et al.*, 2004*a*, 2004*b*), and have been dated at 179 ± 9 Ma (Tribuzio *et al.*, 2004).

Implications for continental rifting and ocean opening

The age determinations reported in this study permit mantle exhumation rates during rift evolution to be estimated. The age of the oldest pelagic sediments associated with the Ligurian Tethys ophiolites (~164 Ma; Chiari *et al.*, 2000; Bill *et al.*, 2001) can be assumed to indicate the timing of mantle exhumation at the sea floor. The pressure at which the studied mantle section cooled below the closure temperature of the Sm–Nd system cannot be constrained precisely. An upper pressure limit of 0·8 GPa is provided by the olivine + plagioclase assemblage in the basic pyroxenites, and a lower pressure limit of ~0·4 GPa is presumed, in agreement with the onset of amphibolite-facies metamorphism at $P \leq 0{\cdot}3$ GPa. These pressure limits suggest uplift of 12–25 km (assuming a rock density value of 3·3 g/cm^3) and integrated exhumation rates between 1·2 and 0·6 mm/year.

Recent studies of modern rifted continental margins have shown that the top of the exhumed mantle consists of a brittle fault zone (e.g. Manatschal, 2004). Continental break-up is inferred to develop through extensional detachment structures that root into the lithospheric mantle. These structures develop at an advanced stage of rift evolution and lead to exhumation of progressively deeper mantle levels (see also Whitmarsh *et al.*, 2001). The ubiquitous brittle structures observed in the mantle bodies of the present study, superimposed on a plagioclase-facies shear zone, are consistent with a shallow detachment fault event (Fig. 13).

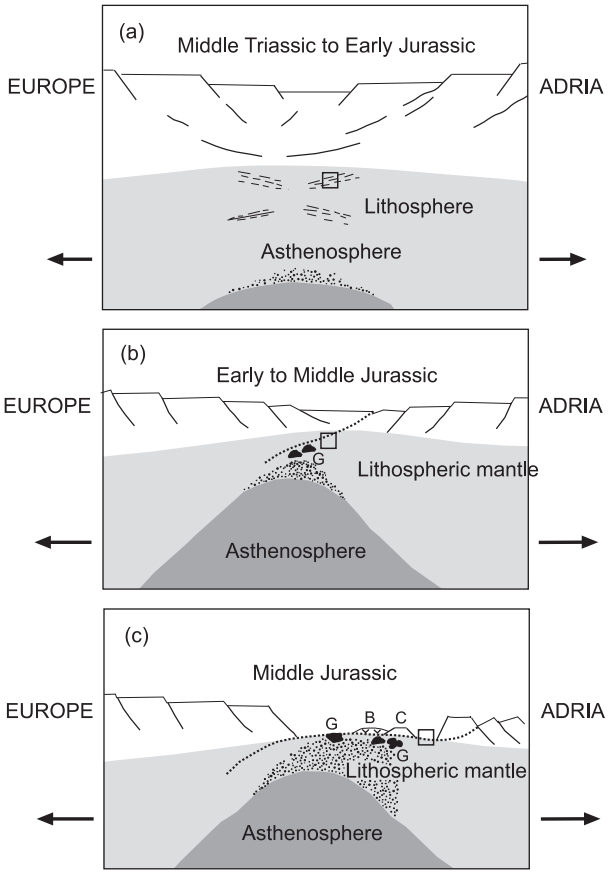

Fig. 13. Schematic reconstruction of the External Liguride mantle evolution during the Mesozoic rifting. The sections are not to scale (see text for further explanation). (a) Lithosphere necking (after Whitmarsh *et al.*, 2001) and development of plagioclase-facies mylonitic shear zones above the ascending asthenosphere. The asthenosphere ascent could be related to melt impregnation at deeper lithospheric mantle levels, as recorded by the southernmost mantle bodies of the External Liguride units (Müntener & Piccardo, 2003). (b) Lithospheric detachment stage: involvement of plagioclase-bearing mylonites in the detachment faulting-related brittle deformation, associated with intrusion of MOR-type syn-rift gabbros (G) (Tribuzio *et al.*, 2004). (c) Continental break-up: mantle denudation before the onset of sea-floor spreading. The MOR-type melts are emplaced as lava flows (locally erupted onto continental crust remnants) and gabbro bodies (Marroni *et al.*, 1998; Montanini & Tribuzio, 2003). Square box indicates garnet pyroxenite-bearing mantle section of this study; stippled area, lithospheric mantle percolated by asthenospheric melts; G, gabbroic bodies; C, continental crust remnants; B, basalt flows.

The plagioclase mylonites from the External Liguride mantle section could have originated along the same extensional detachment that gave rise to the brittle structures. The occurrence of such fine-grained mylonites is known to induce strain softening and reduction of the bulk strength of the lithospheric mantle (Vissers *et al.*, 1995; Frederiksen & Braun, 2001) and to promote further strain localization (Dijkstra *et al.*, 2004). This implies that the Ligurian Tethys rifting was a simple-shear dominated process, which resulted in asymmetric

extension (Lemoine *et al.*, 1987; Vissers *et al.*, 1991). However, most numerical and analogue models of the formation of non-volcanic rifted margins (Brun & Beslier, 1996; Bowling & Harry, 2001; Michon & Merle, 2003), as well as those based on observations from modern and fossil margins (e.g. Whitmarsh *et al.*, 2001), predict an early stage of pure shear-controlled lithospheric necking, in relation to the ascent of the underlying asthenosphere (Whitmarsh *et al.*, 2001). In addition, slow cooling in the plagioclase stability field and the relatively large time interval between plagioclase mylonite formation and the onset of brittle deformation–hydration argues against continuous evolution along a detachment structure. We thus propose that the External Liguride plagioclase mylonites, formed by an extensional shearing event related to a lithospheric necking stage, mark the onset of the rift evolution. Alternatively, the plagioclase-facies shear zone may have marked the boundary between a relatively cold mantle section (e.g. the garnet pyroxenite-bearing peridotites of this study), and the underlying hotter lithospheric mantle heated by asthenospheric melt ascent and infiltration (e.g. the southernmost External Liguride massifs). This hypothesis implies that the mantle impregnation process was already active in Middle to Late Triassic times.

CONCLUSIONS

The fertile mantle section from the External Liguride units (Northern Apennines) was exhumed at an ocean–continent transition. The mantle bodies considered in the present study escaped melt contamination and intrusion and preserve relics of a deep-seated lithospheric history. In particular, garnet-bearing pyroxenite layers record an early stage of equilibration in the subcontinental lithosphere under high P–T conditions ($\sim$2·8 GPa and $\sim$1100°C).

Pyroxenites and enclosing peridotites preserve evidence for a two-stage high-temperature decompression. Garnet-bearing parageneses in the pyroxenites were initially replaced by two pyroxenes + spinel and then by olivine + plagioclase assemblages. The peridotites are characterized by relics of a spinel tectonite fabric extensively overprinted by plagioclase-facies mylonitic deformation. The early decompression, from the garnet to spinel stability field, was associated with cooling to T $\sim$950°C and presumably occurred in relation to Late Variscan (Late Carboniferous to Early Permian) continental extension. The subsequent near-isothermal decompression, including the plagioclase-facies shearing event, was probably related to the onset of the Mesozoic rifting event (i.e. in the Middle to Late Triassic) that led to oceanization in the Middle Jurassic.

The high-temperature decompression was overprinted by a widespread polyphase brittle deformation under decreasing temperature conditions, coupled with hydration. In particular, the brittle evolution includes an early amphibolite-facies stage, followed by low-temperature hydrothermal alteration and serpentinization associated with polyphase cataclasis. The brittle evolution stage is attributed to involvement of the studied mantle section in the footwall of an extensional detachment system. This probably reactivated rheological weaknesses developed under high-temperature, ductile, conditions (i.e. the plagioclase-facies shear zones) and led to continental break-up and mantle exhumation at the sea floor.

ACKNOWLEDGEMENTS

We wish to thank Matteo Beneventi for helping with mineral separation and field assistance. We are also grateful to Gloria Vaggelli for EMP technical assistance, Giuliana De Grandis, Luca Barchi and Andrea Comelli for sample preparation, and Edvige Masini for drawing the maps. Dr Sergei Simakov is acknowledged for helping with P–T calculations. Othmar Müntener and Dante Canil provided constructive comments on the manuscript. Editorial handling and remarks by Colin Devey are also appreciated. This work was supported by funds from the Ministero Italiano dell'Università e della Ricerca (Progetti di Ricerca d'Interesse Nazionale).

REFERENCES

Adam, J., Green, T. H. & Day, R.A. (1992). An experimental study of two garnet pyroxenite xenoliths from the Bullenmerri and Gnotuk Maars of western Victoria, Australia. *Contributions to Mineralogy and Petrology* **111**, 505–514.

Agrinier, P., Mevel, C. & Girardeau, J. (1988). Hydrothermal alteration of the peridotites cored at the ocean/continent boundary of the Iberian margin: petrologic and stable isotope evidence. In: Boillot, G. Winterer, E. L., *et al.* (eds) *Ocean Drilling Program Scientific Results, 103*. College Station, TX: Ocean Drilling Program, pp. 225–233.

Allen, D. E. & Seyfried, W. E.,Jr (2003). Compositional controls on vent fluids from ultramafic-hosted hydrothermal systems at mid-ocean ridges: an experimental study at 400°C, 500 bars. *Geochimica et Cosmochimica Acta* **67**, 1531–1542.

Ai, Y. (1994). A revision of the garnet–clinopyroxene Fe^{2+}–Mg exchange geothermometer. *Contributions to Mineralogy and Petrology* **115**, 467–473.

Alt, J. C. & Shanks, W. C. (1998). Sulphur in serpentinized oceanic peridotites: serpentinization processes and microbial sulfate reduction. *Journal of Geophysical Research* **103**, 9917–9929.

Anczkiewicz, R., Platt, P., Thirlwall, M. F. & Wakabayashi, J. (2004). Franciscan subduction off to a slow start: evidence from high precision Lu–Hf garnet ages on high grade blocks. *Earth and Planetary Science Letters* **225**, 147–161.

Apted, M. J. & Liou, J. G. (1983). Phase relations among greenschist–epidote amphibolite and amphibolite in a basaltic system. *American Journal of Science* **283**, 328–354.

Arnold, J., Jacoby, W. R., Schmeling, H. & Schott, B. (2001). Continental collision and the dynamic and thermal evolution of the Variscan orogenic crustal root—numerical models. *Journal of Geodynamics* **31**, 273–291.

Barrett, J. J. & Spooner, E. F. C. (1977). Ophiolitic breccias associated with allochthonous oceanic crustal rocks in the East Ligurian Apennines, Italy—a comparison with observations from rifted oceanic ridges. *Earth and Planetary Science Letters* **35**, 79–91.

Beccaluva, L., Macciotta, G., Piccardo, G. B. & Zeda, O. (1984). Petrology of lherzolitic rocks from the Northern Apennine ophiolites. *Lithos* **17**, 299–316.

Bedini, R. M., Blichert-Toft, J., Boyet, M. & Albarède, F. (2004). Isotopic constraints on the cooling of the continental lithosphere. *Earth and Planetary Science Letters* **223**, 99–111.

Bernini, M., Vescovi, P. & Zanzucchi, G. (1997). Schema strutturale dell'Appennino settentrionale. *Ateneo Parmense Acta Naturalia* **33**, 43–54.

Bertotti, G. (1991). Early Mesozoic extension and Alpine shortening in the western Southern Alps: the geology of the area between Lugano and Menaggio (Lombardy, Northern Italy). *Memorie della Società Geologica di Padova* **43**, 17–123.

Bertotti, G., Picotti, V., Bernoulli, D. & Castellarin, A. (1993). From rifting to drifting: tectonic evolution of the South-Alpine upper crust from the Triassic to the Early Cretaceous. *Sedimentary Geology* **86**, 53–76.

Bertotti, G., Seward, D., Wijbrans, J., Ter Voorde, M. & Urford, A. J. (1999). Crustal thermal regime prior to, during, and after rifting: a geochronological and modeling study of the Mesozoic South Alpine rifted margin. *Tectonics* **18**, 185–200.

Beslier, M. O., Cornen, G. & Girardeau, J. (1996). Tectonometamorphic evolution of peridotites from the ocean/continent transition of the Iberia Abyssal Plain. In: Sawyer, D. S., Whitmarsh, R. B. Klaus, A., *et al.* (eds) *Ocean Drilling Program Scientific Results, 149*. College Station, TX: Ocean Drilling Program, pp. 397–411.

Bill, M., O'Dogherty, L., Guex, J., Baumgartner, P. O. & Masson, H. (2001). Radiolarite ages in Alpine–Mediterranean ophiolites: constraints on the oceanic spreading and the Tethys–Atlantic connection. *Geological Society of America Bulletin* **113**, 129–143.

Blichert-Toft, J. & Albarède, F. (1997). The Lu-Hf isotope geochemistry of chondrites and the evolution of the mantle-crust system. *Earth Planetary Scence Letters* 148, 243-258.

Blichert-Toft, J., Albarède, F. & Kornprobst, J. (1999). Lu–Hf isotope systematics of garnet pyroxenites from Beni Bousera, Morocco: implications for basalt origin. *Science* **283**, 1303–1306.

Boillot, G., Feraud, G., Recq, M. & Girardeau, J. (1989). Undercrusting by serpentinite beneath rifted margins. *Nature* **6242**, 523–525.

Boland, J. N. & Van Roermund, H. L. M. (1983). Mechanisms of exsolution in omphacites from high-temperature type B eclogites. *Physics and Chemistry of Minerals* **9**, 30–37.

Bonatti, E. & Hamlyn, P.R. (1981). Oceanic ultramafic rocks. In: Emiliani, C. (ed.) *The Sea*. New York: John Wiley, pp. 241–283.

Bowling, J. C. & Harry, D. L. (2001). Geodynamic models of continental extension and the formation of non-volcanic rifted continental margins. In: Wilson, R. C. L., Withmarsh, R. B., Taylor, B. & Froitzheim, N. (eds) *Non-Volcanic Rifting of Continental Margins: a Comparison of Evidence from Land and Sea. Geological Society, London, Special Publications* **187**, 511–536.

Brey, G. P. & Kohler, T. (1990). Geothermometry in four-phase lherzolites II. New thermobarometers, and practical assesment of existing thermobarometers. *Journal of Petrology* **31**, 1353–1378.

Brun, J. P. & Beslier, M. O. (1996). Mantle exhumation at passive margins. *Earth and Planetary Science Letters* **142**, 161–173.

Burg, J. P., Bodinier, J. L., Chaudry, S., Hussain, S. & Dawood, H. (1998). Infra-arc mantle–crust transition and intra-arc mantle diapirs in the Kohistan Complex (Pakistani Himalaya): petro-structural evidence. *Terra Nova* **10**, 74–80.

Caruso, L. & Chernosky, J. V.,Jr (1979). The stability of lizardite. *Canadian Mineralogist* **17**, 757–769.

Chiari, M., Marcucci, M. & Principi, G. (2000). The age of the radiolarian cherts associated with the ophiolites in the Apennines (Italy) and Corsica (France): a revision. *Ofioliti* **25**, 141–146.

Comas, M. C., Sànchez-Gòmez, G., Cornen, E. & de Kaenel, E. (1996). Serpentinized peridotite breccia and olistostromes on basement highs from the Iberia Abyssal Plain: implications for tectonic margin evolution. In: Sawyer, D. S., Whitmarsh, R. B., Klaus, A., *et al.* (eds) *Ocean Drilling Program Scientific Results, 149*. College Station, TX: Ocean Drilling Program, pp. 577–591.

Cornen, G., Beslier, M. & Girardeau, J. (1996). Petrologic characteristics of the ultramafic rocks from the ocean/continent transition in the Iberia Abyssal Plain. In: Sawyer, D. S., Whitmarsh, R. B. & Klaus, A. *et al.* (eds) *Ocean Drilling Program Scientific Results, 149*. College Station, TX: Ocean Drilling Program, pp. 377–395.

Cortesogno, L., Galbiati, B. & Principi, G. (1987). Note alla 'Carta geologica delle ofioliti del Bracco' e ricostruzione della paleogeografia Giurassico-Cretacica. *Ofioliti* **12**, 261–342.

Dalmasso, J., Barci-Funel, G. & Ardison, G. J. (1992). Reinvestigation of the decay of the long-lived odd–odd ^{176}Lu nucleus. *Applied Radiation and Isotopes* **43**, 69–76.

Dal Piaz, G. V. (1993). Evolution of Austro-alpine and Upper Penninic basement in the North-Western Alps from Variscan convergence to post-Variscan extension. In: von Raumer, J. F. & Neubauer, F. (eds) *Pre-Mesozoic Geology in the Alps*. New York: Springer-Verlag, 327–344.

Davies, G. R., Nixon, P. H., Pearson, D. G. & Obata, M. (1993). Tectonic implications of graphitized diamonds from the Ronda peridotite massif, soutrhern Spain. *Geology* **21**, 471–474.

de Ronde, A. A., Heilbronner, R., Stuenitz, H. & Tullis, J. (2004). Spatial correlation of deformation and mineral reaction in experimentally deformed plagioclase–olivine aggregates. *Tectonophysics* **27**, 93–109.

Desmurs, L., Manatschal, G. & Bernoulli, D. (2001). The Steinmann trinity revisited: exhumation and magmatism along an ocean–continent transition: the Platta nappe, eastern Switzerland. In: Wilson, R. C. L., Withmarsh, R. B., Taylor, B. & Froitzheim, N. (eds) *Non-Volcanic Rifting of Continental Margins: a Comparison of Evidence from Land and Sea. Geological Society, London, Special Publications* **187**, 235–266.

Dijkstra, A.H., Drury M.R., Vissers R.L.M., Newman, J. & Van Roermund H.L.M. (2004). Shear zones in the upper mantle: Evidence from alpine- and ophiolite-type peridotite massifs. In: Alsop, G.I., & Holdsworth, R.E. (eds.): Flow processes in Faults and Shear zones. *Geological Society London Special Publication* **224**, 11–24.

Eggins, S. M. (1992). Petrogenesis of Hawaiian tholeiites: 1, phase equilibria constraints. *Contributions to Mineraogy and Petrology* **110**, 387–397.

Ellis, D. J. & Green, D. H. (1979). An experimental study of the effect of Ca upon garnet–clinopyroxene Fe–Mg exchange equilibria. *Contributions to Mineralogy and Petrology* **71**, 13–22.

Evans, B. W., Johannes, W., Otterodoom, H. & Tromsdorff, V. (1976). Stability of chrysotile and antigorite in the serpentine multisystem. *Schweizerische Mineralogische und Petrographische Mitteilungen* **56**, 9–93.

Evans, B.W. (1982). Phase relations of metamorphic amphiboles; natural occurrence and theory; Amphiboles in metamorphosed ultramafic rocks. *Reviews in Mineralogy and Geochemistry* **9B**, 98–113.

Evans, B.W. (2004). The serpentinite multisystem revisited: chrysotile is metastable. *International Geology Review* **46**, 479–506.

Frederiksen, S. & Braun, J. (2001). Numerical modelling of strain localisation during extension of the continental lithosphere. *Earth and Planetary Science Letters* **188**, 241–251.

Frost, B. R. (1985). On the stability of sulfides, oxides and native metals in serpentine. *Journal of Petrology* **26**, 31–63.

Furusho, M. & Kanagawa, K. (1999). Transformation-induced strain localization in a lherzolite mylonite from the Hidaka metamorphic belt of central Hokkaido, Japan. *Tectonophysics* **313**, 411–432.

Ganguly, J., Tirone, M. & Hervig, R. L. (1988). Diffusion kinetics of samarium and neodymium in garnet, and a method for determining cooling rates of rocks. *Science* **281**, 805–807.

Gasparik, T. (1984). Two-pyroxene thermobarometry with new experimental data in the system CaO–MgO–Al_2O_3–SiO_2. *Contributions to Mineralogy and Petrology* **87**, 87–97.

Godard, G. & Martin, S. (2000). Petrogenesis of kelyphites in garnet peridotites: a case study from the Ulten zone, Italian Alps. *Journal of Geodynamics* **30**, 117–145.

Green, D. H. & Ringwood, A. E. (1967). An experimental investigation of the gabbro to eclogite transformation and its petrological applications. *Geochimica et Cosmochimica Acta* **31**, 767–833.

Handy, M. R. & Stünitz, H. (2002). Strain localization by fracturing and reaction weakening—a mechanism for initiating exhumation of subcontinental mantle beneath rifted margins. In: de Meer, S., Drury, M. R., de Bresser, J. H. P. & Pennock, G. M. (eds) *Deformation Mechanisms, Rheology and Tectonics: Current Status and Future Perspectives. Geological Society, London, Special Publications* **200**, 387–407.

Handy, M. R. & Zingg, A. (1991). The tectonic and rheological evolution of an attenuated cross section of the continental crust: Ivrea crustal section, southern Alps, northwestern Italy and southern Switzerland. *Geological Society of America Bulletin* **103**, 236–253.

Hermann, J., Müntener, O. & Günther, D. (2001). Differentiation of mafic magma in a continental crust-to-mantle transition zone. *Journal of Petrology* **42**, 189–206.

Hirschmann, M. M. & Stolper, E. M. (1996). A possible role for garnet pyroxenite in the origin of the garnet signature in MORB. *Contributions to Mineralogy and Petrology* **124**, 185–208.

Holland, T. & Blundy, J. D. (1994). Non-ideal interactions in calcic amphiboles and bearing on amphibole–plagioclase thermometry. *Contributions to Mineralogy and Petrology* **116**, 433–447.

Hoogerduijn Strating, E. H., Rampone, E., Piccardo, G. B., Drury, M. & Vissers, R. L. M. (1993). Subsolidus emplacement of mantle peridotite during incipient oceanic rifting and opening of the Mesozoic Tethys (Voltri Massif, NW Italy). *Journal of Petrology* **34**, 901–927.

Hopkinson, L., Beard, J. S. & Boulter, C. A. (2004). The hydrothermal plumbing of a serpentinite-hosted detachment: evidence from the West Iberia non-volcanic rifted continental margin. *Marine Geology* **204**, 1–15.

Irving, A. J. (1974). Geochemical and high pressure experimental studies on garnet pyroxenite and pyroxene granulite xenoliths from the Delegate basaltic pipes. Australia. *Journal of Petrology* **15**, 1–40.

Jacobsen, S. B. & Wasserburg, G. J. (1980). Sm–Nd isotopic evolution of chondrites. *Earth and Planetary Science Letters* **50**, 139–155.

Joanny, V., Van Roermund, H. L. M. & Lardeaux, J. M. (1991). The clinopyroxene/plagioclase symplectite in retrograde eclogites: a potential geothermobarometer. *Geologische Rundschau* **80**, 303–320.

Johnson, K. T. M. (1998). Experimental determination of partition coefficients for rare earth and high-field-strength elements between clinopyroxene, garnet and basaltic melt at high pressures. *Contributions to Mineralogy and Petrology* **133**, 60–68.

Kennedy, C. S. & Kennedy, G. C. (1976). The equilibrium boundary between graphite and diamond. *Journal of Geophysical Research* **81**, 2467–2470.

Kimball, K.L., & Evans, C.A. (1988). Hydrothermal alteration of peridotite from the Galicia Margin, Iberian Peninsula. In: Boillot, G., Winterer, E. L., et al. (eds) *Ocean Drilling Program Scientific Results*, 103. College Station, TX: Ocean Drilling Program, pp. 241–251.

Klemme, S. (2004). The influence of Cr on the garnet–spinel transition in the Earth's mantle: experiments in the system MgO–Cr_2O_3–SiO_2 and thermodynamic modelling. *Lithos* **77**, 639–646.

Kornprobst, J., Piboule, M., Roden, M. & Tabit, A. (1990). Corundum-bearing garnet clinopyroxenites at Beni Bousera (Morocco): original plagioclase-rich gabbros recrystallized at depth within the mantle? *Journal of Petrology* **31**, 717–745.

Krogh, E. J. (1988). The garnet–clinopyroxene Fe–Mg geothermometer—a reinterpretation of existing experimental data. *Contributions to Mineralogy and Petrology* **99**, 44–48.

Krogh Ravna, E. (2000). The garnet–clinopyroxene Fe^{2+}–Mg geothermometer: an updated calibration. *Journal of Metamorphic Geology* **18**, 211–219.

Lardeaux, J. M. & Spalla, M. I. (1991). From granulites to eclogites in the Sesia zone (Italian Western Alps): a record of opening and closure of the Piedmont ocean. . *Journal of Metamorphic Geology* **9**, 35–58.

Leake, B.E., Woolley, A.R., Arps, C.E.S., Birch, W.D., Gilbert, M.C., Grice, J.D., Hawthorne, F.C., Kato, A., Kisch, H.J., Krivovichev, V.G., Linthout, K., Laird, J., Mandarino, J.A., Maresch, W.V., Nickel, E.H., Rock, N.M.S., Schumacher, J.C., Smith, D.C., Stephenson, N.C.N., Ungaretti, L., Whittaker, E.J.W. & Guo, Y.Z. (1997). Nomenclature of amphiboles: report of the subcommittee on amphiboles of the international mineralogical association, commission on new minerals and mineral names. *American Mineralogist* **82**, 1019–1037.

Lemoine, M., Tricart, P. & Boillot, G. (1987). Ultramafic and gabbroic ocean floor of the Ligurian Tethys (Alps, Corsica, Apennine): in search of a genetic model. *Geology* **15**, 622–625.

Lenoir, X., Garrido, C. J., Bodinier, J. L., Dautria, J. M. & Gervilla, F. (2001). The recrystallization front of the Ronda peridotite: evidence for melting and thermal erosion of subcontinental lithospheric mantle beneath the Alboran Basin. *Journal of Petrology* **42**, 141–158.

Liou, J. G., Kuniyoshi, S. & Ito, K. (1974). Experimental studies of the phase relations between greenschist and amphibolite in a basaltic system. *American Journal of Science* **274**, 613–632.

Ludwig, K. R. (2003). *Isoplot/Ex version 3.0. A Geochronological Toolkit for Microsoft Excel. Berkeley Geochronology Center Special Publication 2003*. 1A, 47.

Manatschal, G. (2004). New models for evolution of magma-poor rifted margins based on a review of data and concepts from West Iberia and Alps. *International Journal of Earth Sciences* **93**, 432–466.

Manatschal, G. & Bernoulli, D. (1999). Architecture and tectonic evolution of nonvolcanic margins: present-day Galicia and ancient Adria. *Tectonics* **18**, 1099–1119.

Manatschal, G., Froitzheim, N., Rubenach, M. & Turrin, B. D. (2001). The role of detcahment faulting in the formation of an ocean–continent transition: insights from the Iberia Abyssal plain. In: Wilson, R. C. L., Withmarsh, R. B., Taylor, B. & Froitzheim, N. (eds) *Non-Volcanic Rifting of Continental Margins: a Comparison of Evidence from Land and Sea. Geological Society, London, Special Publications* **187**, 405–428.

Marroni, M., Molli, G., Montanini, A. & Tribuzio, R. (1998). The association of continental crust rocks with ophiolites in the Northern Apennines (Italy): implications for the continent–ocean transition in the Western Tethys. *Tectonophysics* **292**, 43–66.

Marroni, M., Molli, G., Montanini, A., Ottria, G., Pandolfi, L. & Tribuzio, R. (2002). The External Ligurian units (Northern Apennine, Italy): from rifting to convergence of a fossil ocean–continent transition zone. *Ofioliti* **27**, 119–131.

Martini, I.P., Rau, A. & Tongiorgi, M. (1986). Syntectonic sedimentation in a Middle triassic rift, Northern Apennines, Italy. *Sedimentary Geology* **47**, 191–219. .

McCandless, T. E. & Gurney, J. J. (1989). Sodium in garnet and potassium in clinopyroxene: criteria for classifying mantle eclogites. In: Ross, J. (ed.) *Kimberlites and Related Rocks. Special Publication of the Geologiacal Society of Australia* **2**, 827–832.

Meli, S., Montanini, A., Thoni, M. & Frank, W. (1996). Age of mafic granulite blocks from the External Liguride Units (northern Apennine, Italy). *Memorie di Scienze Geologiche di Padova* **48**, 65–72.

Messiga, B. & Bettini, E. (1990). Reactions behaviour during kelyphite and symplectite formation: a key study of mafic granulites and eclogites from the Bohemian Massif. *European Journal of Mineralogy* **2**, 125–144.

Mével, C. (2003). Serpentinization of abyssal peridotites at mid-ocean ridges. *Comptes Rendus de l'Académie des Sciences* **335**, 825–852.

Michon, L. & Merle, O. (2003). Mode of lithospheric extension: conceptual models from analogue modelling. *Tectonics* **22**, 1028. doi 10.1029/2002TC001435

Montanini, A. (1997). Mafic granulites in the Cretaceous sedimentary mélanges from the northern Apennine (Italy): petrology and tectonic implications. *Schweizerische Mineralogische und Petrographische Mitteilungen* **77**, 43–64.

Montanini, A. & Tribuzio, R. (2001). Gabbro-derived and felsic granulites from the Northern Apennines (Italy): evidence for emplacement of tholeiitic basalts in the post-Variscan lower crust. *Journal of Petrology* **42**, 2259–2277.

Montanini, A. & Tribuzio, R. (2003). Igneous to metamorphic evolution of mafic rocks from a fossil ocean–continent transition (External Liguride ophiolites, Italy). *Geophysical Research Abstracts* **5**, EAE03-A-06549.

Montanini, A., Tribuzio, R., Beneventi, M. & Bersani, D. (2005). Insights into the origin of mantle graphite from a new occurence in garnet pyroxenites from the External Liguride peridotites (Northern Apennine, Italy). Peridotite Workshop 2005, Lanzo (Torino) 27–30 September. *Ofioliti* **30**, 200.

Morishita, T. & Arai, S. (2003). Evolution of spinel–pyroxene symplectite in spinel-lherzolites from the Horoman Complex, Japan. *Contributions to Mineralogy and Petrology* **144**, 509–522.

Müntener, O. & Hermann, J. (1996). The Val Malenco lower crust–upper mantle complex and its field relations (Italian Alps). *Schweizerische Mineralogische und Petrographische Mitteilungen* **763**, 475–500.

Müntener, O. & Hermann, J. (2001). The role of lower crust and continental upper mantle during formation of nonvolcanic passive margins: evidence from the Alps. In: Wilson, R. C. L., Withmarsh, R. B., Taylor, B. & Froitzheim, N. (eds) *Non-Volcanic Rifting of Continental Margins: a Comparison of Evidence from Land and Sea. Geological Society, London, Special Publications* **187**, 267–288.

Müntener, O. & Piccardo, G. B. (2003). Melt migration in ophiolites: the message from Alpine–Apennine peridotites and implications for embryonic ocean basins. In: Dilek, Y. & Robinson, P. T. (eds) *Ophiolites in the Earth History. Geological Society, London, Special Publications* **218**, 69–89.

Müntener, O., Hermann, J. & Trommsdorff, V. (2000). Cooling history and exhumation of lower crustal granulite and upper mantle (Malenco, eastern Central Alps). *Journal of Petrology* **41**, 175–200.

Müntener, O., Pettke, T., Desmurs, L., Meier, M. & Schaltegger, U. (2004). Refertilization of mantle peridotite in embryonic ocean basins: trace element and Nd-isotopic evidence and implications for crust–mantle relationships. *Earth and Planetary Science Letters* **221**, 293–308.

Newman, J., Lamb, W. M., Drury, M. R. & Vissers, R. L. M. (1998). Deformation processes in a peridotite shear zone: reaction-softening by an H_2O-deficient, continuous net transfer reaction. *Tectonophysics* **303**, 193–222.

Nickel, K. G. (1986). Phase equilibria in the system SiO_2–MgO–Al_2O_3–CaO–Cr_2O_3 (SMACCR) and their bearing on spinel/garnet lherzolite relationships. *Neues Jahrbuch für Mineralogie, Abhandlungen* **155**, 259–287.

Niida, K. & Green, D. H. (1999). Stability and chemical composition of pargasitic amphibole in MORB pyrolite under upper mantle conditions. *Contributions to Mineralogy and Petrology* **135**, 18–40.

Obata, M. (1994). Material transfer and local equilibria in a zoned kelyphite from a garnet pyroxenite, Ronda, Spain. *Journal of Petrology* **35**, 271–287.

O'Brien, P. J. (1997). Garnet zoning and reaction textures in overprinted eclogites, Bohemian Massif, European Variscides: a record of their thermal history during exhumation. *Lithos* **41**, 119–133.

O'Hanley, D. S. (1996). *Serpentinites*. Oxford: Oxford University Press, 277 pp.

O'Hanley, D. S., Chernovsky, J. V.,Jr & Wicks, F. J. (1989). The stability of lizardite and chrysotile. *Canadian Mineralogist* **27**, 483–493.

O'Hara, M. J., Richardson, S. W. & Wilson, G. (1971). Garnet-peridotite stability and occurrence in crust and mantle. *Contributions to Mineralogy and Petrology* **32**, 48–68.

O'Neill, H. S. C. (1981). The transition between spinel lherzolite and garnet lherzolite, and its use as a geobarometer. *Contributions to Mineralogy and Petrology* **77**, 185–194.

Palandri, J. L. & Reed, M. H. (2004). Geochemical models of metasomatism in ultramafic systems: serpentinization, rodingitization and sea floor carbonate chimney precipitation. *Geochimica et Cosmochimica Acta* **68**, 1115–1133.

Pearson, D. G. & Nixon, P. H. (1996). Diamonds in young orogenic belts: graphitised diamonds from Beni Bousera, N. Morocco, a comparison with kimberlite-derived diamond occurrences and implications for diamond genesis and exploration. *African Geosciences Review* **3**, 295–316.

Pearson, D. G. & Nowell, G. M. (2004). Re–Os and Lu–Hf isotope constraints on the origin and age of pyroxenites from the Beni Bousera Peridotite Massif: implications for mixed peridotite–pyroxenite mantle sources. *Journal of Petrology* **45**, 439–455.

Pearson, D. G., Davies, G. R. & Nixon, P. H. (1993). Geochemical constraints on the petrogenesis of diamond facies pyroxenites from the Beni Bousera peridotite massif, North Morocco. *Journal of Petrology* **34**, 125–172.

Peltonen, P., Kinnunen, K. A. & Huhma, H. (2002). Petrology of two diamondiferous eclogite xenoliths from the Lahtojoki kimberlite pipe, eastern Finland. *Lithos* **63**, 151–164.

Peressini, G., Mazzucchelli, M., Rivalenti, G. & Hoffmann, A. W. (2004). Triassic emplacement of the External Gabbro Unit of the Finero mafic complex: U–Pb SHRIMP zircon ages and their implication for the Ivrea–Verbano zone, Western Italian Alps. *Geophysical Research Abstracts* **6**, 05072.

Pertermann, M. & Hirschmann, M. M. (2003). Anhydrous partial melting experiments on MORB-like eclogite: phase relations, phase compositions and mineral–melt partitioning of major elements at 2–3 GPa. *Journal of Petrology* **44**, 2173–2201.

Peters, T. (1968). Distribution of Mg, Fe, Al, Ca and Na in coexisting olivine, orthopyroxene and clinopyroxene in the Totalp serpentinite (Davos, Switzerland) and in the Alpine metamorphosed Malenco serpentinite (N. Italy). *Contributions to Mineralogy and Petrology* **18**, 65–75.

Piccardo, G. B. (1976). Petrologia del massiccio lherzolitico di Suvero (La Spezia). *Ofioliti* **1**, 279–317.

Piccardo, G. B., Rampone, E. & Vannucci, R. (1990). Upper mantle evolution during continental rifting and ocean formation: evidence from peridotite bodies of the Western Alpine–Northern Apennine system. *Mémoires de la Société Géologique de France* **156**, 326–333.

Piccardo, G. B., Müntener, O., Zanetti, A. & Pettke, T. (2004a). Ophiolitic peridotites of the Alpine–Apennine system: mantle processes and geodynamic relevance. *International Geological Review* **46**, 1119–1159.

Piccardo, G. B., Müntener, O. & Zanetti, A. (2004b). Alpine–Apennine ophiolitic peridotites: new concepts on their composition and evolution. *Ofioliti* **26**, 193–200.

Poggi, E., Piccardo, G. B. & Zanetti, A. (2005). Melt percolation and impregnation in peridotites from a fossil rifted margin: evidence from the Mt. Nero peridotite (External Ligurides, Northern Apennine, Italy). *Geophysical Research Abstracts* **7**, 00464.

Rampone, E. & Piccardo, G. B. (2000). The ophiolite–oceanic lithosphere analogue: new insights from the Northern Apennines (Italy). In: Dilek, J., Moores, E., Elthon, D. & Nicolas, A. (eds) *Ophiolites and Oceanic Crust: New Insights from Field Studies and Ocean Drilling Program. Geological Society of America Special Papers* **349**, 21–34.

Rampone, E., Piccardo, G. B., Vannucci, R., Bottazzi, P. & Ottolini, L. (1993). Subsolidus reactions monitored by trace element partitioning: the spinel- to plagioclase-facies transition in mantle peridotites. *Contributions to Mineralogy and Petrology* **115**, 1–17.

Rampone, E., Hoffmann, A. W., Piccardo, G. B., Vannucci, R., Bottazzi, P. & Ottolini, L. (1995). Petrology, mineral and isotope geochemistry of the External Liguride peridotites (northern Apennines, Italy). *Journal of Petrology* **36**, 81–105.

Rampone, E., Romairone, A., Abouchami, W., Piccardo, G. B. & Hoffmann, A. W. (2005). Chronology, petrology and isotope geochemistry of the Erro–Tobbio peridotites (Ligurian Alps, Italy): records of Late Palaeozoic lithospheric extension. *Journal of Petrology* **46**, 799–827.

Ricci, C. A. & Serri, G. (1975). Evidenza geochimica sulla diversa affinità petrogenetica delle rocce basiche comprese nella serie a facies toscana. *Bollettino della Società Geologica Italiana* **94**, 1187–1198.

Röhm, A. H. E., Snieder, R., Goes, S. & Trampert, J. (2000). Thermal structure of continental upper mantle inferred from S-wave velocity and surface heat flow. *Earth and Planetary Science Letters* **181**, 395–407.

Salters, V. J. M. & Dick, H. J. B. (2001). Mineralogy of the mid-ocean-ridge basalt source from neodymium isotopic composition of abyssal peridotites. *Nature* **418**, 68–72.

Scherer, E. E., Cameron, K. L. & Blichert-Toft, J. (2001). Lu–Hf garnet geochronology: closure temperature relative to the Sm–Nd system and the effects of trace mineral inclusions. *Geochimica et Cosmochimica Acta* **64**, 3414–3432.

Schmidt, M.W. & Poli, S. (1998). Experimentally based water budgets for dehydrating slabs and consequences for arc magma generation. *Earth and Planetary Science Letters* **163**, 361–379.

Schott, B. & Schmeling, H. (1998). Delamination and detachment of a litospheric root. *Tectonophysics* **296**, 225–247.

Sibson, R. H. (1987). Earthquake rupturing as a mineralizing agent in hydrothermal systems. *Geology* **15**, 701–704.

Simakov, S. (2006). Redox state of eclogites and peridotites from subcratonic upper mantle and a connection with diamond genesis. *Contributions to Mineralogy and Mineralogy,* **151**, 282–296.

Simakov, S. & Taylor, L. A. (2000). Geobarometry for mantle eclogites: solubility of Ca-Tschermak in clinopyroxene. *International Geological Review* **42**, 534–544.

Skelton, A. D. L. & Valley, J. W. (2000). The relative timing of serpentinization and mantle exhumation at the ocean–continent transition, Iberia: constraints from oxygen isotopes. *Earth and Planetary Science Letters* **178**, 127–138.

Snow, J. E., Schmidt, G. & Rampone, E. (2000). Os isotopes and highly siderophile elements (HSE) in the Ligurian ophiolites, Italy. *Earth and Planetary Science Letters* **175**, 119–132.

Stähle,V., Frenzel, G., Michard A. & Schneider, W. (1990). Zircon syenite pegmatites in the Finero peridotite (Ivrea zone): evidence for a synite from a mantle source. Earth Planet. Sci. Lett. **101**, 196–205.

Stähle, V., Frenzel, G., Hess, J.C., Saupé, F., Schmidt, S.Th. & Schneider, W. (2001). Permian metabasalts and Triassic alkaline dykes in the northern Ivrea Zone: clues to the post-Variscan geodynamic evolution of the Southern Alps. Schweizerische Mineralogische und Petrographische Mitteilungen, 81, 1–21.

Taylor, L. A. & Neal, C. R. (1989). Eclogites with oceanic crustal and eclogites, Udachnaya kimberlite pipe, Yakutia, Siberia: evidence of mantle signatures from the Bellsbank kimberlite, South Africa, Part I: Mineralogy, petrography and whole-rock chemistry. *Journal of Geology* **118**, 91–100.

Terranova, R. & Zanzucchi, G. (1984). Relationships between ophiolites and flysch sequences in the Mt. Penna–Mt. Ragola area. *Ofioliti* **6**, 287–292.

Thirlwall, M. F. & Anczkiewicz, R. (2004). Multidynamic isotope ratio analysis using MC–ICP–MS and the causes of secular drift in Hf, Nd and Pb isotope ratios. *International Journal of Mass Spectroscopy* **235**, 9–81.

Thompson, R. N. (1974). Some high-pressure pyroxenes. *Mineralogical Magazine* **39**, 768–787.

Treves, B. E. & Harper, G. D. (1994). Exposure of serpentinites on the ocean floor; sequence of faulting and hydrofracturing in the Northern Apennine ophicalcites. In: Principi, G. (ed.) *Sedimentary Cover of Ophiolitic and Oceanic Sequences. Ofioliti* **19**, 435–466.

Tribuzio, R., Thirlwall, M. F. & Messiga, B. (1999). Petrology, mineral and isotope geochemistry of the Sondalo gabbroic complex (Central Alps, Northern Italy): implications for the origin of post-Variscan magmatism. *Contributions to Mineralogy and Petrology* **136**, 48–62.

Tribuzio, R., Tiepolo, M. & Vannucci, R. (2000). Evolution of gabbroic rocks from the Northern Apennine ophiolites (Italy): comparison with the lower oceanic crust from modern slow-spreading ridges. In: Dilek, J., Moores, E., Elthon, D. & Nicolas, A. (eds) *Ophiolites and Oceanic Crust: New Insights from Field Studies and Ocean Drilling Program. Geological Society of America, Special Papers* **349**, pp. 129–138.

Tribuzio, R., Thirlwall, M. & Vannucci, R. (2004). Origin of the gabbro–peridotite association form the Northern Apennine ophiolites (Italy). *Journal of Petrology* **45**, 1109–1124.

Tribuzio, R., Montanini, A. & Thirlwall, M. F. (2005). Geochemistry of garnet pyroxenite layers from the External Liguride mantle peridotites (Northern Apennine, Italy): evidence for recycling of crustal material in a ophiolitic mantle sequence. Peridotite Workshop 2005, Lanzo (Torino), 27–30 September. *Ofioliti* **30**, 222.

Tumiati, S., Thöni, M., Nimis, P., Martin, S. & Mair, V. (2003). Mantle–crust interactions during Variscan subduction in the Eastern Alps (Nonsberg–Ulten zone): geochronology and new petrological constraints. *Earth Planetary Science Letters* **210**, 509–526.

Ulmer, P. & Trommsdorff, V. (1999). Phase relations of hydrous mantle subducting to 300 km. In: Fei, Y., Bertka, C.M. & Mysen, B.O. (eds) *Mantle Petrology: Field Observations and High Pressure Experimentation: A Tribute to Francis R. Boyd, Geochemical Society Special Publication* **6**, 259–281.

Van der Wal, V. & Vissers, R. L. M. (1996). Structural petrology of the Ronda peridotite, SW Spain: deformation history. *Journal of Petrology* **37**, 23–43.

Van Orman, J. A., Grove, T. L., Shimizu, N. & Layne, G. D. (2002). Rare earth element diffusion in a natural pyrope single crystal at 2·8 GPa. *Contributions to Mineralogy and Petrology* **142**, 416–424.

Villa, I. M., Hermann, J., Müntener, O. & Trommsdorff, V. (2000). ^{39}Ar–^{40}Ar dating of multiply zoned amphibole generations (Malenco, Italian Alps). *Contributions to Mineralogy and Petrology* **140**, 363–381.

Vissers, R. L. M., Drury, M. R., Hoogerduijn Strating, E. H. & Van der Wal, D. (1991). Shear zones in the upper mantle: a case of study in an Alpine lherzolite massif. *Geology* **19**, 990–993.

Vissers, R. L. M., Drury, M. R., Hoogerduijn, S, trating, E. H., Spiers, C. J. & van der Wal, D. (1995). Mantle shear zones and their effect on lithosphere strength during continental breakup. *Tectonophysics* **249**, 155–171.

Voshage, H., Hofmann, A. W., Mazzucchelli, M., Rivalenti, G., Sinigoi, S., Raczek, I. & Demarchi, G. (1990). Isotopic evidence from the Ivrea Zone for a hybrid lower crust formed by magmatic underplating. *Nature* **347**, 731–736.

Webb, S. A. C. & Wood, B. J. (1986). Spinel–pyroxene–garnet relationship and their dependence on Cr/Al ratio. *Contributions to Mineralogy and Petrology* **92**, 471–480.

Wells, P. R. A. (1977). Pyroxene thermometry in simple and complex systems. *Contributions to Mineralogy and Petrology* **62**, 129–139.

White, A. J. R. (1964). Clinopyroxenes from eclogites and basic granulites. *American Mineralogist* **49**, 883–888.

Whitmarsh, R. B., Manatschal, G. & Minshull, T. A. (2001). Evolution of magma-poor continental margins from rifting to seafloor spreading. *Nature* **413**, 150–154.

Yaxley, G. M. & Brey, G. P. (2003). Phase relations of carbonate-bearing eclogite assemblages from 2·5 to 5·5 GPa: implications for petrogenesis of carbonatites. *Contributions to Mineralogy and Petrology* **146**, 606–619.